공학석사 학위논문

Analysis of the parameters affecting LiDAR intensity and its application in determining rock joint surface alteration

라이다 반사 강도의 영향 인자 분석과

암반 변질도 산정에의 적용

2020 년 8 월

서울대학교 대학원

에너지시스템공학부

김 문 주

Analysis of the parameters affecting LiDAR intensity and its application in determining rock joint surface alteration

지도 교수 전 석 원

이 논문을 공학석사 학위논문으로 제출함

2020 년 6 월

서울대학교 대학원

에너지시스템공학부

김 문 주

김문주의 공학석사 학위논문을 인준함

2020 년 7 월

위 원 장 민 기 복 (인)

부위원장 전 석 원 (인)

위 원 송 재 준 (인)

Abstract

Analysis of the parameters affecting LiDAR intensity and its application in determining rock joint surface alteration

Moonjoo Kim

The Graduate School

Department of Energy Systems Engineering

Rock Mechanics & Rock Engineering Laboratory

Seoul National University

Rock mass characterization is required in many rock engineering projects. Among the parameters used to determine the rock mass rating (RMR), the discontinuity of rock mass, which includes the separation and weathering of the discontinuity surfaces, accounts for the largest share. In another method of classifying rock mass, the Geological Strength Index (GSI), the joint alteration factor (J_a), which also indicates the discontinuity condition of rock mass such as the weathering of the discontinuity and the state of the filling, has a greater influence than any other parameters. There is a tendency lately for the classification of rock mass, which have previously been carried out in a variety of manual ways, to be automated due to the development of photogrammetry and light detection and ranging (LiDAR) technologies. For characterizing rock mass using LiDAR, qualities of rock discontinuities such as joint spacing, waviness, smoothness, and alteration should be determined. Estimating joint spacing, waviness, and smoothness factor by

LiDAR have been studied using quantitative point cloud coordinates, but the task of estimating the joint alteration factor is more subjective. As previously mentioned, the effect of the joint alteration factor on the overall GSI is large. This study examines accurate approach for determining joint alteration factor from LiDAR intensity data, which is the return strength of the laser pulse that generated the point.

Previous studies have found that the reflective percentages or intensity of LiDAR are high for hard and less weathered rocks and small for more weathered and weak rocks. Therefore, through a number of laboratory experiments, a method of determining the joint alteration factor using LiDAR intensity was formulated by analyzing the factors directly affecting LiDAR. Factors that were not directly related to rock weathering were corrected. Laboratory experiments were performed to assess the impact of the scanning distance, incidence angle, roughness, micro-roughness, RGB color values, water saturation, and the mechanical properties of the rock on the LiDAR intensity and to ascertain how they affect it. As a result, it was concluded that the direct relationship between LiDAR intensity and the joint alteration factor could be obtained by correcting the scan distance, incidence angle, and RGB color values, which are the most influential factors to the LiDAR intensity when determining the joint alteration factor.

The separation of a discontinuity and the type of filling material also have a significant influence on the J_a and on LiDAR intensity and this was what the laboratory experiment was also designed to measure. The separation was increased from 1 mm to 6 mm at 1 mm interval to measure the change in intensity. Bentonite and sand were used as a filling material to examine how they affected the intensity. As a result of the experiment, it was concluded that it was possible to estimate which and how much filling material existed through the degree of the change in the intensity in the separation or in the filling position.

A comparison of the hand-mapped data of rock alteration and the LiDAR intensity at three sites of rock slope also indicated a good relationship between intensity and joint alteration factor. The LiDAR intensity was high in the case of rock mass that was estimated to have a large GSI joint alteration factor or discontinuity condition within the RMR by means of hand mapping, and the degree to which this

was the case was more apparent after correction on distance, incidence angle, and RGB value. Although correcting for each point would be the ideal, it would take significant time and effort. Consequently, for convenient and quick rock mass classification, the average value of the scanning distance, the incidence angle, or the RGB can be used alternatively.

Keywords: LiDAR, intensity, joint surface, alteration, point cloud, rock mass classification.
Student ID: 2018-24350

Contents

Lists of Tables

Lists of Figures

Chapter 1. Introduction

1.1 Background

Rock mass characterization is required in many projects in rock engineering practices including excavation design, support design, and stope design, among others. To date, manual mapping methods such as scanline survey and window mapping performed by experts have been widely used to obtain the engineering characteristics of rock discontinuities. However, large-scale mines, tunnels, and slopes often require the collection of large amounts of data at design or construction sites. In such cases, collecting large amounts of data on rock characteristics is time consuming and likely to include both operator safety issues and operator biases. In order to solve these problems, various methods of research have been conducted to find ways to obtain this information safely, quickly but precisely. Recently, the development of optical technologies has meant that the use of LiDAR (Light Detection and Ranging), which enables the fast and accurate acquisition of 3D point cloud information, has rapidly increased (Abellan et al., 2014).

Cai et al. (2004, 2007) quantified the Geological Strength Index (GSI: Hoek et al., 1998), one of the methods of classifying rock, using four indices that determine the block volume, waviness, smoothness, and degree of alteration. Waviness and smoothness are roughness factors. GSI has been widely used by determining its parameters by visual observation. However, the latest LiDAR equipment is rapidly improving its specifications, ensuring the precision and accuracy required to effectively obtain information on rock at site. The use of LiDAR is considered to be applicable to the determination of the rock classification index. Among the indices proposed by Cai et al. (2004, 2007) for quantification, block volume, waviness, and

smoothness have been assessed using LiDAR in previous studies (Lee et al., 2017). In addition, Lee et al. (2016) obtained the joint attitude from LiDAR data.

In this regard, the intensity of the reflection of the LiDAR shows the strength of the reflected signal. As 3D coordinates and intensity are acquired at the same time, LiDAR intensity can be used as adequate data for understanding and analyzing the properties of the indicators. The scanned laser beam is reflected and recorded in the sensor. Since LiDAR in topographic surveys uses a laser in the near-infrared wavelength region, its intensity contains information about the state of the surface, regardless of the condition of the weathering in most cases. However, the number of studies that have been conducted on the characteristics, calibration, and utilization of LiDAR's intensity data are still insufficient.

Therefore, a laboratory experiment on the various factors affecting the reflection strength, that is, the intensity, of LiDAR was conducted and an index of the joint alteration factor based on the results was created to apply to local rock mass.

1.2 Previous researches

1.2.1 GSI system for rock mass classification

GSI is a rock mass classification method that can be utilized only through visual observation. Cai et al. (2004, 2007) quantified the GSI (Hoek et al., 1998) by determining the block volume, waviness, smoothness, and alteration factor of joints. Lee et al. (2017) considered LiDAR to be applicable for the calculation of rock classifications such as the GSI, as the latest LiDAR equipment is rapidly improving in terms of its specifications, precision, and accuracy. The characterization of rock mass is required for many applications, and for these purposes, it is necessary to obtain design input parameters such as deformation moduli and strength parameters

for numerical modeling. Although such parameters can ultimately be determined from in situ tests, at the preliminary design stage, when underground access is limited, the practical way to obtain these parameters is to apply a rock mass classification system to characterize the rock mass and estimate the rock mass properties. Over the years, many classification systems, such as RQD, Rock Mass Rating, Q and GSI systems, have been developed.

Among them, the Q system is widely used for rock support system design and the GSI system is used for estimating design parameters. The GSI system is the only rock mass classification system that is directly linked to engineering parameters such as the Mohr–Coulomb and Hoek–Brown strength parameters or rock mass modulus. However, the established application of the GSI system is hindered by the fact that the use of the system is to some extent subjective and requires long-term experience.

Consequently, Cai et al. (2004) developed a quantitative approach to assist in the use of the GSI system. “It employs the block volume and joint condition factor as quantitative characterization factors. The approach is built upon the link between descriptive geological terms and measurable field parameters such as joint spacing and joint roughness. The newly developed approach adds quantitative means to facilitate the use of the system, especially by inexperienced engineers.”

The GSI values are obtained from the block volume and joint condition factor, which, in turn, are determined from site construction documents and field mapping data. Based on the GSI values and intact rock strength properties, equivalent Mohr–Coulomb strength parameters and the elastic modulus of the jointed rock mass are calculated and compared to in situ test results. The point estimate method is implemented to approximate the mean and variance of the mechanical properties of the jointed rock masses. It is evident that both the means and variances of the strength and deformation parameters predicted by the GSI system are in firm agreement with the field test data. Figure 1.1 shows the quantification of GSI in table.

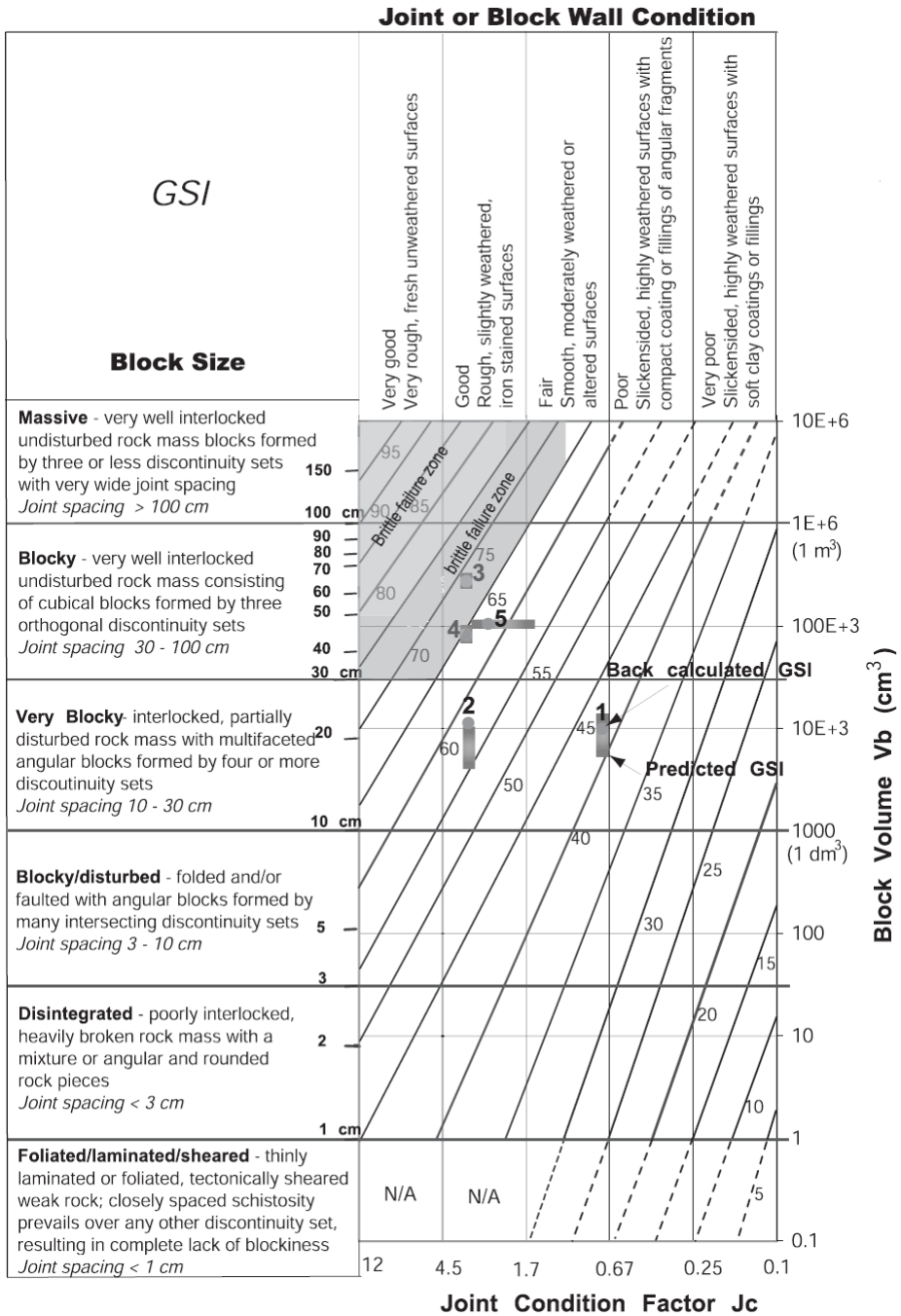

Figure 1.1 Quantification of GSI chart (Cai et al., 2004)

To this end, the joint condition factor is obtained through the multiplication of the large-scale waviness and small-scale smoothness divided by the joint alteration factor like Equation 1.1.

$$J_C = \frac{J_W J_S}{J_A} \tag{1.1}$$

As the joint alteration factor is considered to be just one measure in many different fields which have different levels of alteration, this measure is difficult to obtain accurately through LiDAR data. Knowing the accurate joint alteration degree is important to calculating the joint condition factor as the joint alteration factor ranges from 0.75 to 12 as shown in Table 1.1. The joint alteration factor can multiply the joint condition factor by more than 10 times.

To consider every detail of the joint alteration factor, including the degree of weathering or type of filling material, in a large site is considered to be almost impossible. Therefore, in most cases, the joint alteration factor is generally considered to be 1 and sometimes 2. Although it is true that rock mass with a joint alteration factor of 8-12 is not common, it is also not accurate to assume that the joint alteration factor is always at relatively low levels.

Cai et al. (2004) showed that the joint alteration factor alone has the largest impact upon the joint condition factor as it can reduce it by more than one order of magnitude. An inaccurate joint alteration factor affects the joint condition factor and, therefore, the calculated GSI will be considered to be inaccurate as a whole.

Table 1.1. Ratings for the joint alteration factor J_a (Cai et al., 2004)

	Term	Description	J_A
Rock wall contact	*Clear joints*		
	Healed or "welded" joints (unweathered)	Softening, impermeable filling (quartz, epidote, etc.)	0.75
	Fresh rock walls (unweathered)	No coating or filling on joint surface, except for staining	1
	Alteration of joint wall: slightly to moderately weathered	The joint surface exhibits one class higher alteration than the rock	2
	Alteration of joint wall: highly weathered	The joint surface exhibits two classes higher alteration than the rock	4
	Coating or thin filling		
	Sand, silt, calcite, etc.	Coating of frictional material without clay	3
	Clay, chlorite, talc, etc.	Coating of softening and cohesive minerals	4
Filled joints with partial or no contact between the rock wall surfaces	Sand, silt, calcite, etc.	Filling of frictional material without clay	4

Table 1.1 Rating for the joint alteration factor J_a (Cai et al., 2004) (Continued)

	Compacted clay materials	"Hard" filling of softening and cohesive materials	6
	Soft clay materials	Medium to low over-consolidation of filling	8
	Swelling clay materials	Filling material exhibits swelling properties	8-12

1.2.2 Relationship between the degree of weathering and LiDAR intensity

Yoo et al. (2015) have suggested a weathering index derived from LiDAR reflectance results. The term "reflectance" was used in their study instead of "intensity" as they used the RIEGL VZ-400 model, which obtains reflectance. The impact of scanning distance or incidence angle could have been minimized through the use of this LiDAR as it receives direct reflectance. Intensity varies with many factors like distance, reflectance, and incidence angle. Laboratory and field tests were conducted to quantitatively analyze and calculate the degree of weathering, which is one of the engineering characteristics of the excavation surface, using a laser scanner with high-resolution imaging technology.

The original reflectance was correlated with the weathering degree of the rock, but consistency was not observed, and it was judged that this was because the reflectance was affected not only by the degree of weathering but also by the object's color. The change in the RGB value for achromatic color was correlated with the reflectance, defined by a linear equation, and a correction equation that considered

the effect of the achromatic RGB value was proposed. The corrected reflectance was found to be closely related to the weathering degree of the rock, and it was considered that it could be used as a more direct indicator of the weathering degree of the rock than the original reflectance result. The weathering index was presented so that the range of the corrected reflectance conformed to the six levels of rock weathering observed by the naked eye.

The proposed calibration formula in this study was verified by comparing the results before and after calibration using scanning data acquired in the actual field. As a result of the verification, it was confirmed that the weathering degree index calculated through the corrected reflectance value showed extremely similar results to the predominant weathering degree and weathering ratio observed in the field.

Ercoli et al. (2013) found the reflectivity of a laser scanner could be used for measuring the degree of weathering of old architecture. As Italy, where the study was conducted, has many aged structures including cultural assets, using a “Schmidt hammer” is not ideal as it may destroy the structure. For this reason, the degree of weathering of the building materials and natural stones is generally quantified, as the decrement of some mechanical features can be measured experimentally by means of compression tests or point load tests in the laboratory or Schmidt hammer tests carried out in situ. Such destructive or damaging tests are unacceptable in cases of cultural heritage since even small amounts of damage must be avoided. This study demonstrated a correlation between the Schmidt hammer rebound values and the reflectivity that was detected by means of terrestrial scanner laser; therefore, it permits the assessing of the degree of weathering of buildings or stones in situ. Accordingly, the results demonstrate that such an investigation could be a significant alternative as an innovative and non-destructive technique.

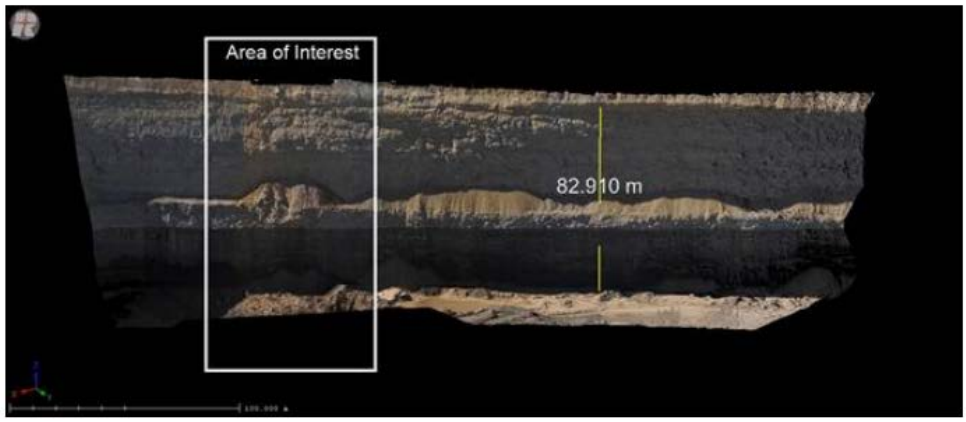

(a)

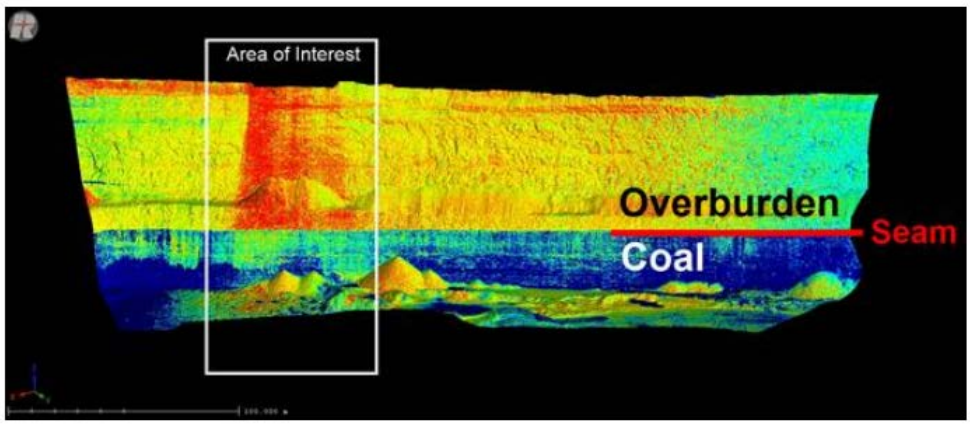

(b)

Figure 1.2 Coal mine high wall mesh (a) Colorized by close range photogrammetry (b) Colorized by relative reflectance of LiDAR (Fowler et al., 2011)

Fowler et al. (2011) found that the advanced detection of weathering and a significant advancement in material classification could be conducted via LiDAR reflectance. These state-of-the-art technologies can be applied in the geological field as well.

It is possible to discern a slight change in the colorization of the wall shown in the boxed area of interest in Figure 1.2 (a). However, further inspection by LiDAR

(Riegl VZ-400) revealed that the area of interest is highlighting a highly reflective material shown in red, whereas the surrounding area is seen in yellow. In this way, the area of interest demonstrates that fresh rock can be extensively discerned through LiDAR reflectance data.

1.3 Objectives

As discussed in the previous section, LiDAR intensity can be used to calculate the degree of alteration in rock mass. Consequently, the primary objectives of this study consist of the following.

The first objective is to ascertain what factors directly affect LiDAR intensity and the degree to which they affect it. Through previous studies, it is evident that scanning distance, incidence angle, saturation, and RGB are factors that influence LiDAR intensity. However, the previous studies were not ideal for field applications. For example, correcting the RGB value of LiDAR intensity only occurred in the field of achromatic color. In this study, experiments are conducted to quantitatively obtain the relationship between not only distance, incidence angle, RGB, degree of saturation, but also roughness, the mechanical properties of rocks (uniaxial compressive strength [UCS], $V_p, V_s,$ porosity), mineral composition, and LiDAR intensity. Additional experiments are also conducted to obtain the relationship between separation, filling material, and LiDAR intensity.

The second objective is to obtain the joint alteration factor by correcting the LiDAR intensity obtained from the local rock mass. The LiDAR intensity and hand-mapped data for three places with different degrees of weathering and joint alteration factors are compared. Finally, I suggest an index of LiDAR intensity in order to estimate the joint alteration factor as closely as possible.

Chapter 2. LiDAR Technology

.

2.1 Characteristics of LiDAR

LiDAR is a remote sensing/measurement tool developed to obtain the precise three-dimensional coordinates of a target by measuring the distance from the sensor to the target by measuring the time a laser beam takes to return. LiDAR is also referred to as LADAR (LAser Detection And Ranging) and Airborne Laser Scanning (ALS) because it is usually loaded onto an aircraft to acquire the data. LiDAR is an active sensor, therefore, it is not normally affected by shadows or clouds and can still fly in bad weather. In addition, LiDAR is able to supplement the shortcomings of optical sensors because it can obtain a large amount of data in a short time and has a high data processing speed. LiDAR basically estimates distance by reflecting the light from the target through pulses of near-infrared light (wavelengths of approximately 900 to 1100 nm and 1500 nm). Due to its ability to aim laser light and short wavelengths from 905 to 1550 nm, LiDAR's infrared spatial resolution can be divided into 0.1° increments. Conversely, the wavelength of the radar (4 mm for 77GHz) has difficulty analyzing small features as the distance increases. (Kim et al., 2012)

Using a 3D scanner, the laser can be projected onto an object, and the shape information of the object can be obtained and converted into digital information. With this 3D scanning technology, extremely small objects such as bolts and nuts can be analyzed, and it is even possible to easily acquire the shape information of a large object such as a building, bridge, or area of terrain. The shape information obtained from the 3D scanner is now being actively used in the field of quality control for comparing production results against their design through detailed

surveys of manufactured products such as reverse engineering and ships required for various industries. Traditionally, in order to obtain the shape information of a specific product, the target product was measured manually by using a tool, but this method takes considerable work and time and there are limitations to the level of accuracy that can be achieved. LiDAR is also used for analysis or accident reproduction in crime scene investigations and is used as basic data for digitally preserving historical artifacts such as cultural properties and restoring them when they are damaged by earthquakes.

The configuration of the LiDAR sensor system is sometimes very complicated depending upon the application field, but the basic configuration is simply divided into a laser transmitter, a laser detector, a signal collection and processing section, and a section for transmitting and receiving data. In addition, the LiDAR sensor can be utilized in a time-of-flight (TOF) method and a phase-shift method according to the modulation method of the laser signal. In the TOF method, it is possible to measure the distance by measuring the time when the reflected pulse signals from objects within the measurement range arrive at the receiver. The phase-shift method is a method that calculates time and distance by emitting a laser beam continuously modulated with a specific frequency and measuring the amount of phase shifts of the signal reflected back from an object within the measurement range. As a laser light source, laser light sources with a specific wavelength or a variable wavelength are used in a wavelength ranging from 250 nm to 11 μm, and recently, semiconductor laser diodes capable of small and low power have been frequently used. In particular, the wavelength of the laser directly affects its permeability of the atmosphere, clouds and rain. The wavelength also affects eye safety. Basically, the power of the laser, wavelength, spectral characteristics, pulse width and shape, receiver sensitivity and dynamic range, and the characteristics of the optical filter and lens are the main factors that determine LiDAR performance. In addition, field of view (FOV), which

indicates the measurement angle of the receiver, the field stop for selecting the measurement range, and the FOV overlap of the laser beam and the receiver are also important items. The minimum time for collecting the unit data with respect to the luminous flux is a factor that determines the range resolution, therefore, data collection and processing within a few nanoseconds is required for a distance resolution of 1 m or less.

Beam divergence is considered to be one of the important specifications of LiDAR. The term is used for aerial LiDAR. Unlike a true laser system, the trajectories of photons in a beam emitted from a LiDAR instrument deviate slightly from the beam propagation line (axis) and form a narrow cone rather than the thin cylinder typical of true laser systems. The beam divergence refers to the increase in the beam diameter that occurs as the distance between the laser instrument and a plane that intersects the beam axis increases. Typical beam divergence settings range from 0.1 to 1.0 millirad. At 0.3 millirad, the diameter of the beam at a distance of 1000 m from the instrument is approximately 30 cm (Figure 2.1). Because the total amount of pulse energy remains constant regardless of the beam divergence, the pulse energy is spread over a larger area with a larger beam divergence, leading to a lower signal-to-noise ratio. (Gatziolis and Andersen, 2008)

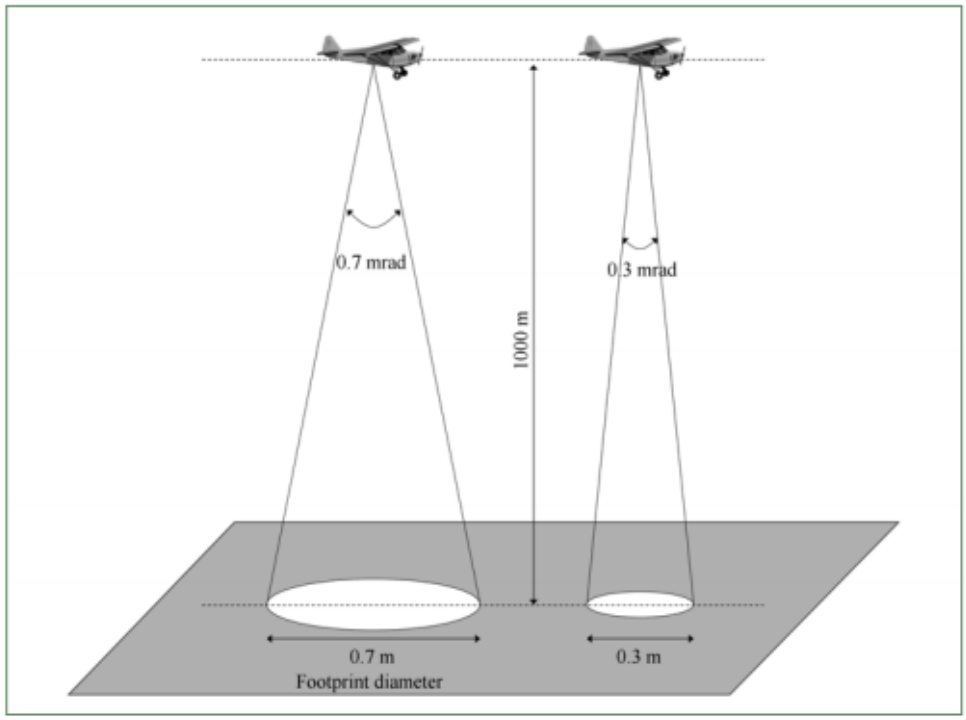

Figure 2.1 Illustration of LiDAR beam divergence (Gatziolis and Andersen, 2008)

The FOV of the LiDAR system refers to the angle which is covered by a sensor. For LiDAR applications, this is equal to the angle at which the LiDAR signals are emitted. For some LiDAR sensors, the number of LiDAR signals emitted per scan cycle (going back and forth) is always the same. In such cases, reducing the angle will result in a denser point pattern, while increasing the FOV spreads the LiDAR returns further apart.

If a camera is used in conjunction with the LiDAR sensor, it is common practice to choose the FOV so that the LiDAR returns will match the area covered by the aerial images. Other factors such as objects on the ground or surface properties can require the FOV to be adjusted accordingly. A dense forest canopy, for instance, may require a wider FOV to obtain some ground returns. At the same time, cities with

high buildings and narrow streets might benefit from a narrower angle to obtain returns from street level.

Table 2.1 shows the specifications of widely used LiDAR models.

Table 2.1. Specification of LiDAR models

Sensor	Range (m)	Scan freq. (Hz)	Range resolution (mm)	Range Accuracy (mm)	Beam divergence (mm x mrad)	Field of view	Wave length (mm)
Dynascan SLM 150/500	150/ 500	10	10	N/A	2.5 x 0.2	360	905
Dynascan S250	250	20	10	10	2.5 x 0.2	360	905
Optech V200	200	80-200	N/A	±50	0.5	360	1064
Optech M1	200	80-200	N/A	±50	0.5	360	1064
Riegl VQ-250	500	-100	N/A	10	7.0 x 0.35	360	1550
Riegl VQ-450	800	-200	N/A	8	7.0 x 0.3	360	1550
Velodyne HDL-64ES2.1	120	5-20	N/A	20	2.0	360 x 31.5	905
Velodyne HDL-32E	70	10	N/A	20	2.79	360 x 40	905
FARO Photon 120	153	61	0.07	2	3.3 x 0.16	320	785

Table 2.1. Specification of LiDAR models (Continued)

FARO Focus 3D	153	97	0.07	2	3.0 x 0.16	305	905
FARO Focus X330	330	97	0.07	2	2.25 x 0.19	300	1550
Z+F Imager 5010C	187	50	0.1	2	3.5 x 0.3	320	1500
Z+F Profiler 9012	119	50-200	0.1	0.9	1.9 x 0.5	360	1500

2.2 LiDAR Intensity

Intensity is a measure, collected for every point, of the return strength of the laser pulse that generated the point. It is based, in part, on the reflectivity of the object struck by the laser pulse. The intensity of the laser pulse reaching the receiver is recorded as a digital number (DN) in the LiDAR recording device. In a study by Coren et al. (2006), the DN recorded can be defined as the ratio of the number of photons reaching the receiver to the number of photons scanned at a given point in time, which physically denotes the strength. Therefore, it can be said that the laser pulse DN is converted into a linear relationship with the number of photons reached. The intensity of the DN can be considered to be mainly changed by factors such as the reflectance of the target, atmospheric transmittance, and the scanning distance.

The reflectivity is a function of the wavelength used, which is most common in the near-infrared spectrum. The strength of the return varies with the composition of the surface object that is reflecting the return.

Intensity is used as an aid in feature detection and extraction, in LiDAR point classification, and as a substitute for aerial imagery when none is available. Burton et al. (2013) clarified that the most important physical factors that influence intensity are distance and target reflectivity, with incidence angle and roughness being secondary.

Shin (2007) and Kaasalainen et al. (2009) organized LiDAR intensity as depicted in Equation (2.1).

$$P_r = \rho \frac{M^2 {D_r}^2 {D_{tar}}^2}{4R^2(R\gamma + D)} P_T \tag{2.1}$$

Equation (2.1) shows that the intensity of the laser reaching the receiver (P_r) is related to target reflectance (ρ), atmospheric transmittance (M), receiver caliber (D_r), target diameter (D_{tar}), scanning distance (R), laser divergence (γ), the laser aperture (D), and the strength of the original laser (P_T). As R is relatively much larger than D, Equation (2.1) can be changed to Equation (2.2). The intensity of Faro laser scanner has range of 0 to 2047. Intensity does not have an unit.

$$P_r = \rho \frac{M^2 {D_r}^2 {D_{tar}}^2}{4R^2\gamma^2} P_T \tag{2.2}$$

However, the incident area of the laser beam and the area of the target can be assumed to be same. If the system specifications or the atmospheric conditions during shooting are fixed, the factors affecting the reflected intensity of the laser are, in particular, the reflectance and scanning distance.

The intensity of the LiDAR point clouds can be used for numerous applications including feature detection and point cloud classification, land cover classification, identifying wet areas in forested areas, or vegetation classification. Junttila et al. (2018) identified the effects of drought on growth and the equivalent water thickness of plants from LiDAR laser intensity features using FARO X330.

Burton et al. (2011) showed a linear relationship between LiDAR intensity and mineral composition. Intensity was proportional to the sum of quartz, plagioclase, and K-feldspar. Clay composition was inversely proportional to intensity.

Pesci et al. (2006) used the intensity of the laser to map and identify multiple layer units exposed upon the walls of a volcanic crater. According to the research, the intensity was closely related to the physical and chemical properties of the reflective object. They also noted that stratigraphic studies using LiDAR intensity can be extended to areas other than volcanic environments. Bellian et al. (2005)

studied the detection of rock deformation using intensity along with other properties. Klise et al. (2009) showed that intensity and multiscan stacking can easily distinguish gravel from sand. Another recent study showed an inverse linear correlation between strength and the clay content (percentage of hydrogen weight) in rocks dominated by carbonate (Franceschi et al. 2009). All these studies point to LiDAR intensity as a potential technique for identifying the characteristics of rock mass. Consequently, understanding the obvious relationship between rock properties and strength could significantly increase the value of LiDAR data in outcrop studies.

Chapter 3. Experimental work

3.1 Method Overview

As demonstrated in early studies, the degree of weathering of a rock mass and the LiDAR intensity data are highly correlated. In this paper, several laboratory experiments were conducted first to ascertain the exact correlation. The relationships between the intensity and the other factors affecting intensity were calculated. The relationships between intensity and distance, incidence angle, saturation, color value (RGB), roughness, micro-roughness, and mechanical properties were measured. In addition, by using the granite and cement mortar specimens, the change in intensity according to the separation of a discontinuity and the type of filling material was also examined.

3.2 Laboratory experiments

3.2.1 Specimens used

A total of 12 rock or rock-like test specimens were used. In this study, a variety of rocks with different properties and colors were prepared: five types of sandstone (Bandera, Berea, Buff Berea, Boise, and Briarhill), two granites, two shales with different anisotropy, limestone, cement mortar, and diastone. All of them were shaped as Brazilian disc, and the size and mechanical properties are presented in Table 3.1.

Table 3.1. Specification of rock specimens

Specimen	Diameter (mm)	Height (mm)	UCS (MPa)	Specific gravity	Porosity (%)	V_S (km/s)	V_p (km/s)
Briarhill	53.5	21.7	12.0	2.1	18.7	1.7	2.6
Buff Berea	53.8	21.5	44.6	2.0	21.8	1.4	2.0
Berea	53.8	23.2	46.0	2.1	18.4	1.6	2.4
Bandera	53.7	23.2	27.6	2.0	23.1	1.6	2.4
Boise	53.7	24.1	29.0	1.8	28.1	1.7	2.7
Granite - 1	50.7	22.6	145.5	2.6	0.8	2.7	5.1
Granite - 2	50.6	24.1	92.9	2.6	0.8	2.9	5.0
Shale - 1	37.9	23.5	191.8	2.8	0.4	3.2	5.5
Shale - 2	37.9	24.1	231.9	2.8	0.1	3.3	6
Limestone	36.3	23.3	56.3	2.7	0.4	2.5	5.0
Cement	54.1	21.7	51.0	2.0	13.1	2.1	4.1
Diastone	53.5	23.4	40.5	1.5	27.9	1.3	2.9

Two sets of these 12 samples were prepared to investigate the relationship between the saturation degree and LiDAR intensity. One sample group was used after 24 hours of saturation in water, the "w-" group; while the other sample group was dried for 24 hours, the "d-" group. Even in the case of a saturated sample, water may evaporate during an experiment, resulting in a decrease in saturation. Thus, just before the experiment, the surfaces of the dry and saturated samples were sprayed with water, and the same experiment was repeated.

Figure 3.1 Dry and wet rock specimen used for experiment

In Figure 3.1, the 12 specimens on the left are dried and the 12 on the right are saturated. Their rock types are as written. Shale-1 has 45˚of anisotropic direction and shale-2 has 90˚ of anisotropic direction. Granite-1 and granite-2 basically have similar properties except for the UCS.

The same experiment was repeated at 5 m, 10 m, 15 m, and 20 m intervals of distance between the specimen and the LiDAR to determine the relationship between the scanning distance and the intensity. To determine the relationship between the incidence angle and the intensity, the sample plate was inclined at 15º intervals from 15º to 90º of dip angle for each distance. A clinometer was used to establish the angle. A slope with a dip angle of 90º has 0º as its incidence angle and a slope with a 15º dip angle has an incidence angle of 75º.

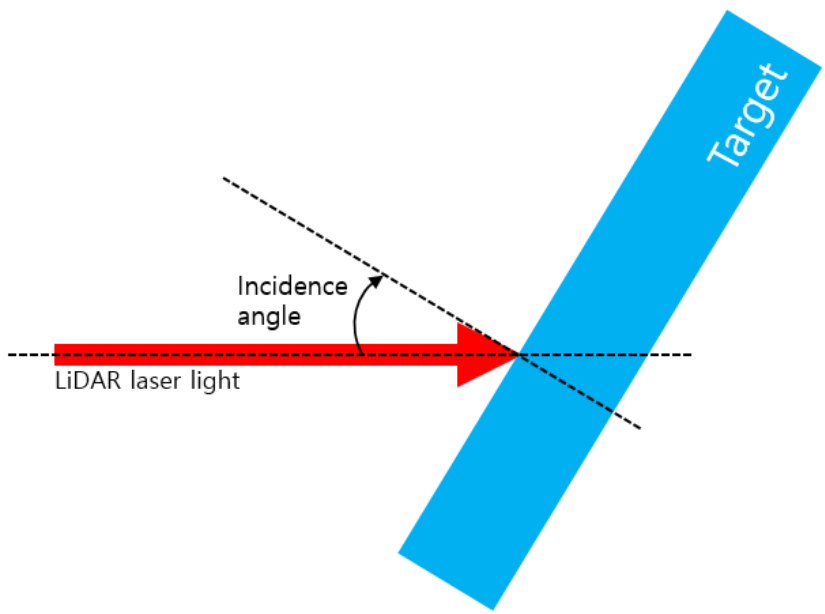

Figure 3.2 Incidence angle

For the relationship between the joint roughness coefficient (JRC) and intensity, samples with JRCs of 4, 8, 12, 16, and 20 were 3D printed. Considering that the point spacing for measuring the intensity was small, approximately 2 mm, it seemed that a large range of roughness such as JRC might not significantly affect the intensity. For this reason, specimens with different levels of fine roughness were created using sandpaper and the change in intensity was measured. This fine roughness was called micro-roughness.

The 3D printer is a device for producing 3D stereoscopic sculptures. The model used for this experiment was a ZPrinter450 by Z Corporation. The 3D printer manufactures moldings by stacking three-dimensional moldings with a layer of about 100 μm thickness using gypsum powder and liquid binder (binding material) provided by Z Corporation. The maximum moldable size is 200 mm X 200 mm X 200 mm. Figure 3.3 and Figure 3.4 describe features of roughness specimen.

The specific method used to build the specimens was adopted from the previous research (Lee et al., 2017). In order to obtain the various target roughnesses of JRC 4, 8, 12, 16, and 20 at equal intervals, a method of changing the Z-coordinate amplitude in the point group information obtained from the artificial joint surface was used.

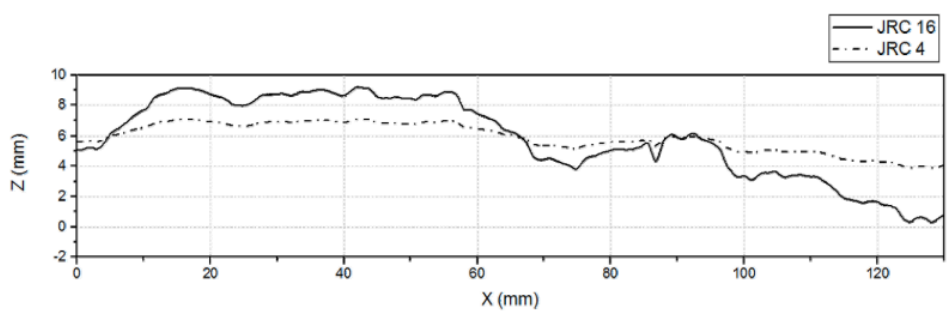

Figure 3.3 Example of roughness profile adjustment (Lee et al., 2017)

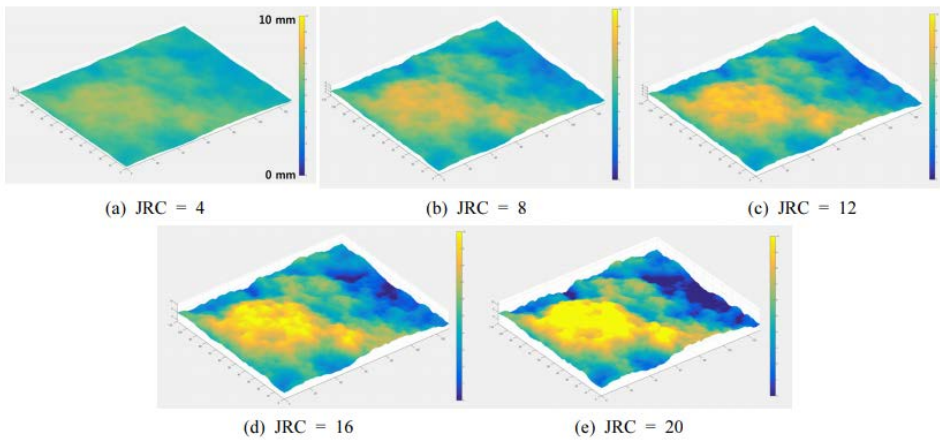

Figure 3.4 Point cloud of gypsum specimen surfaces with five different levels of roughness (Lee et al., 2017)

Five samples with different JRCs; three sandpapers with grit sizes of 40, 100, and 220; and three diastones polished with the sandpaper were placed on a single plate, and the intensity was measured for each distance and each incidence angle. Figure 3.4 shows height of gypsum specimen 3D printed with different JRC.

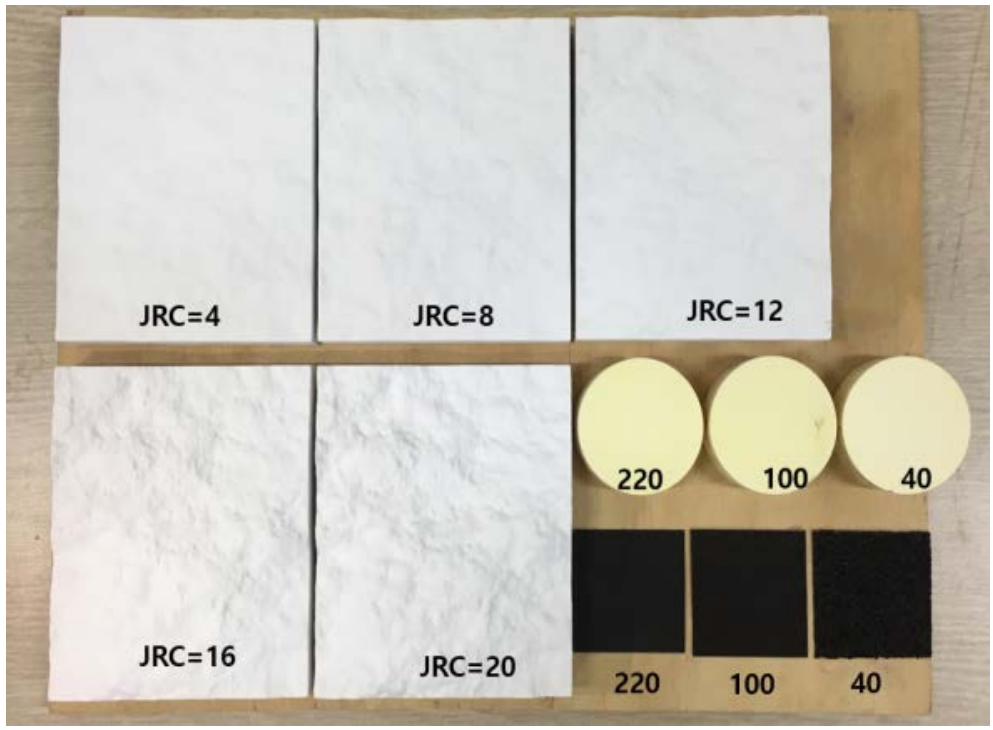

Figure 3.5 Gypsum specimens printed by 3d printer have different JRCs of 4, 8, 12, 16, and 20. Sandpaper with 220, 100, 40 grits (from the left) and diastone polished with the sandpaper were also attached above the sandpaper

In addition, in this study, a laboratory color test was performed to minimize the effects of sunshine and atmospheric conditions in order to identify the characteristics of the RGB values that affect the intensity. A test was performed on the printed paper by setting a total of 252 RGB values. The RGB table was printed and attached to the steel structure to scan with LiDAR.

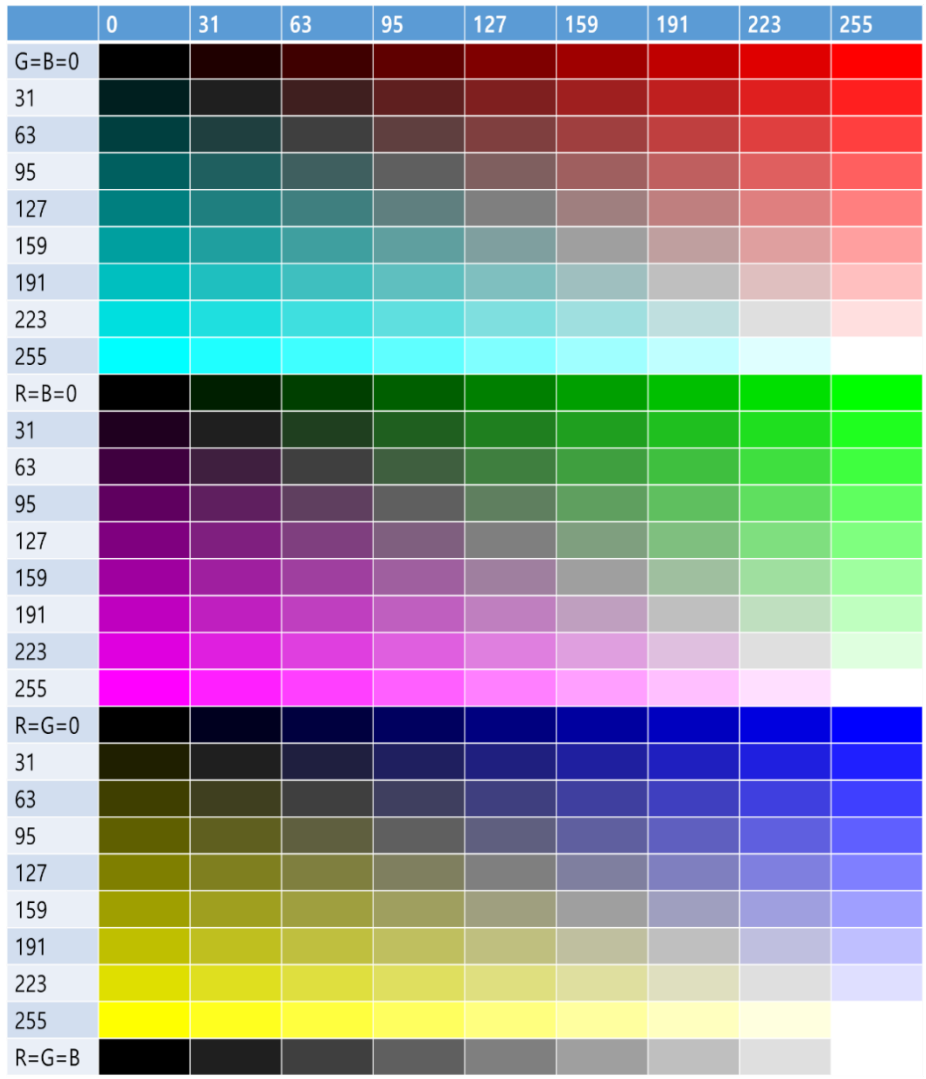

Figure 3.6 Table composed of 252 RGB values

To ascertain the relationship between the separation and intensity, a cuboid cement mortar and a granite sample were prepared and tested with a gap of 1 mm, 2 mm, 3 mm, 4 mm, 5 mm, and 6 mm. Cement mortar and granite samples were also used to find the relationship between the type of filling and the intensity. The fillings used were sand, wet sand, bentonite, and wet bentonite.

Figure 3.7 Cement mortar specimen (in the left) and granite specimen (in the right) filled with sand at 5mm thickness

The bentonite used was Tixoton Standard from Sud-Chemie (Clariant Korea) and the sand was from Joomoonjin Silica Sand Co., Ltd.

3.2.2 Specification of the LiDAR used

The FARO Laser Scanner Focus S350 was used for the experiment. First, the rock specimen test was conducted as follows. The specimen was placed on a table that present in a Figure 3.8 (b) and the LiDAR was installed in front at a certain distance. The first experiment was performed by placing a rock specimen and an RGB color table on hardboard on the table. After all the distances and angles were completed, the experiment was conducted again by placing the JRC and micro-roughness samples on the steel structure along with the rock specimens using the same method and spraying water on the surface of the rock specimens.

In the experiments to investigate the effect of the gap, a specimen piece was placed on a desk and the LiDAR was installed approximately 1.9 m in front of the desk. In the experiments to ascertain the effect of the fillings, rock samples with fillings were placed on the floor, and the LiDAR was installed as shown in Figure 3.8 (a).

(a)

Figure 3.8 The experiment was conducted in the hallway and Room 329-1 of Seoul National University Building #38, 3rd floor (a) Experiments with fillings, (b) Experiments with rock specimen, roughness, and RGB

Figure 3.8. The experiment was conducted in the hallway (a) Experiments with fillings, (b) Experiments with rock specimen, roughness, and RGB (Continued)

The specifications of the LiDAR equipment used in the experiment were as presented in Table 3.2.

For processing all the point clouds, FARO SCENE 2018 software was used.

Table 3.2. Specifications of FARO S350

Item	Specification
Unambiguity Interval	614 m for up to 0.5 million points/sec 307 m at 1 mil pts/sec
Max. Measurement Speed (mil. pts/sec)	Up to 1
Ranging Error (mm)	±1
Angular Accuracy	19 arcsec for vertical/horizontal angles
3D Point Accuracy	2 @ 10 m, 3.5 @ 2 5m
Color Resolution	Up to 165-megapixel color
Field of View (FOV)	300˚vertical / 360˚horizontal
Max. Scan Speed	97 Hz (vertical)
Laser Class	Laser Class 1
Wavelength	1550 nm
Beam Divergence	0.3 mrad (1/e)
Beam Divergence at Exit	2.12 mm (1/e)
Dimensions / Weight	230 x 183 x 103 mm / 4.2 kg(including battery)

Chapter 4. Results and Discussion

4.1 Relationship between LiDAR intensity and related variables

4.1.1 Distance

Since the scanning distance greatly affects the LiDAR intensity, when determining the degree of weathering, it is necessary to correct the influence of the scanning distance. In this study, the experiment was repeated at different scanning distances of 5 m, 10 m, 15 m, and 20 m to obtain the relationship. The results are summarized as follow.

Theoretically, LiDAR intensity is inversely proportional to the square of the scanning distance as shown in Equation (2.1). However, in this study, the intensity tended to increase with increases in distance from 5 m to 15 m. Studies by Tan and Chang (2015) and Kaasalainen et al. (2011) also demonstrated the same tendency as the intensities near 0 m distance are caused by the system noise that is always present in near-distance measurements. Accordingly, this observation may have been resulted from the effects of the unknown amplification of the received optical power or near-distance reducers.

Subsequently, the equation in which intensity was inversely proportional to the scanning distance at a distance of 15 m or more was used for correction. When correcting for a distance of 15 m or less, the experimental results were used as they are in Figure 4.1. Forty, 100, and 220 in Figure 4.1 (a) refer to the number of particles in a unit area (1cm x 1cm), which can be understood as the grit size of the sandpaper.

As a result of the experiments, a distance of at least 15 m was concluded to be suitable to obtain the most accurate intensity data. The legend of Figure 4.1 (a) is the grit size and the legend of Figure 4.1 (b) shows type of specimen.

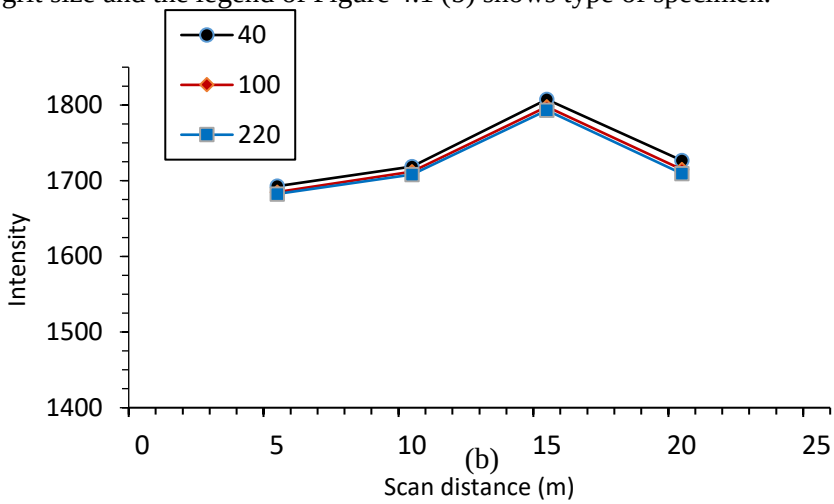

(a)

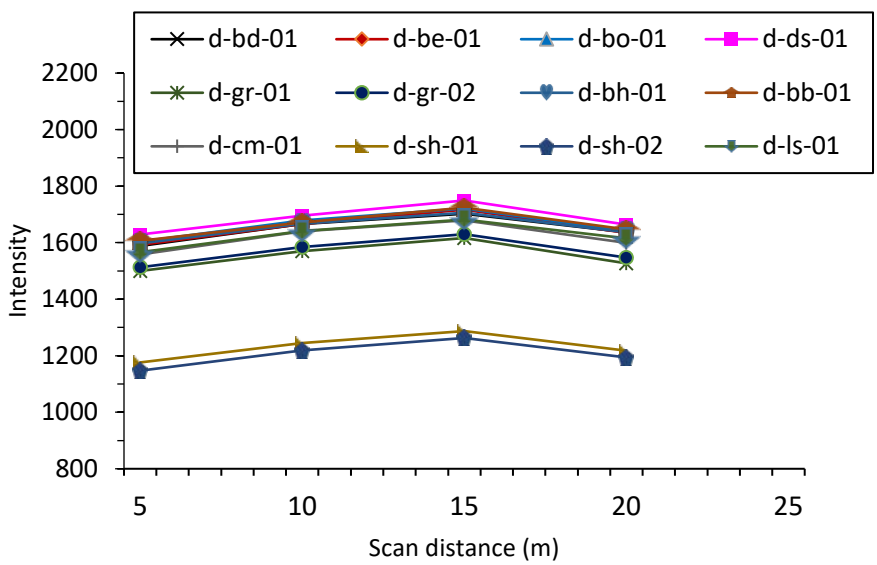

(b)

Figure 4.1 Relationship between scanning distance and intensity (a) Diastone with micro-roughness with incidence angle of 15˚, (b) Rock specimens with incidence angle of 45˚

4.1.2 Incidence angle

In order to observe how the intensity of LiDAR laser varies depending upon the incidence angle on the surface of the object, the intensity was measured after the sample was placed at various dip angles using a clinometer. The dip angle was adjusted from 15˚ to 90˚, which corresponds to 75˚ to 0˚degrees of the incidence angle as shown in Figure 3.2. The results are presented in Figure 4.2.

The intensity of the sample from 0˚ to 75˚ of the incidence angle linearly decreased, and there was a difference in the intensity value of approximately 250 in all the samples as shown in Figure 4.2. Considering that the intensity of the FARO S350 equipment measures from 0 to 2047, the difference in the intensity was more than 10 % of the full range which can not be ignored. However, in the case of the shale specimen with an anisotropic angle of 90˚ (sh90), the intensity difference according to the incidence angle of the dry sample was 486. In the case of the saturated sample, the difference was approximately 250, similar to the other samples. Therefore, it was judged that the value of the dry shale-2 samples were outliers that may have emerged because of the anisotropic angle. The legend of Figure 4.2 shows specimen ID.

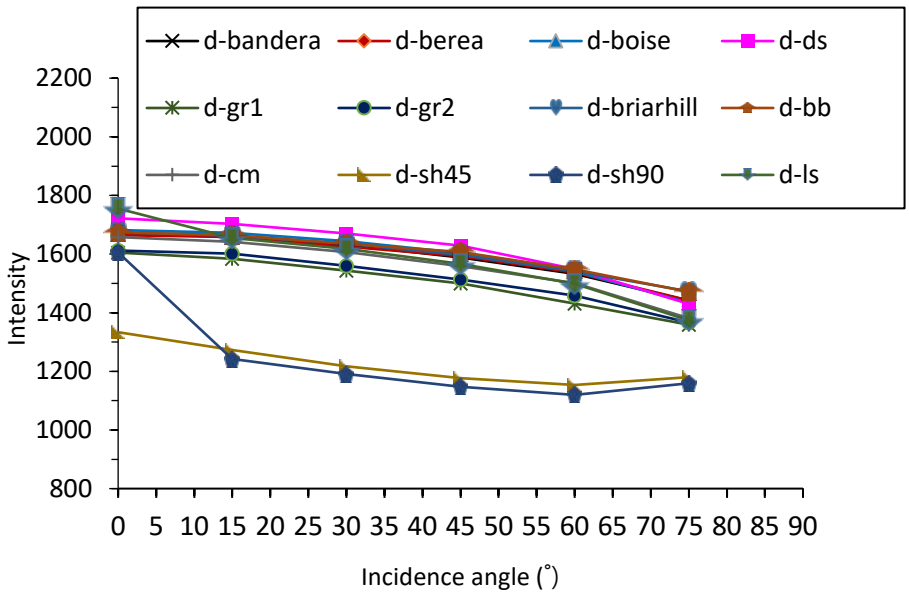

(a)

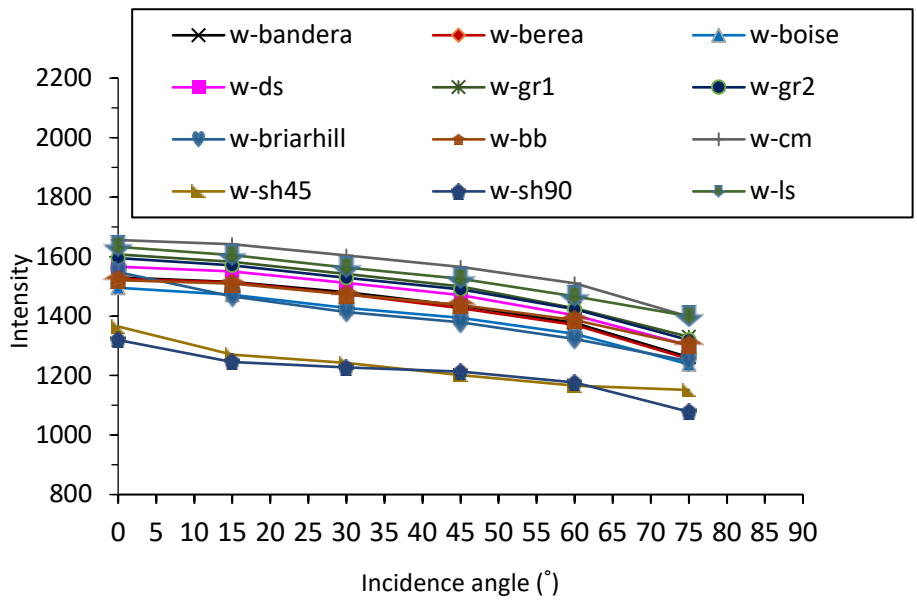

(b)

Figure 4.2 Relationship between incidence angle and intensity at 5m distance (a) Dry rock specimen, (b) Wet rock specimen

4.1.3 JRC

In order to examine the relationship between roughness and intensity, samples with different JRCs were 3D printed. The specific steps undertaken to produce the specimens were explained in Chapter 3.2.1.

Samples with JRCs of 4, 8, 12, 16, and 20 were attached to a wooden board and tested as in Figure 3.8 (b). The experiment results are presented in Figure 4.3.

Through this, it was observed that the change in intensity according to the change in the JRC was negligible as it was up to 50 in just one case and almost the same for most of the other cases. Therefore, it was concluded that the roughness of the JRC scale did not alter the LiDAR intensity.

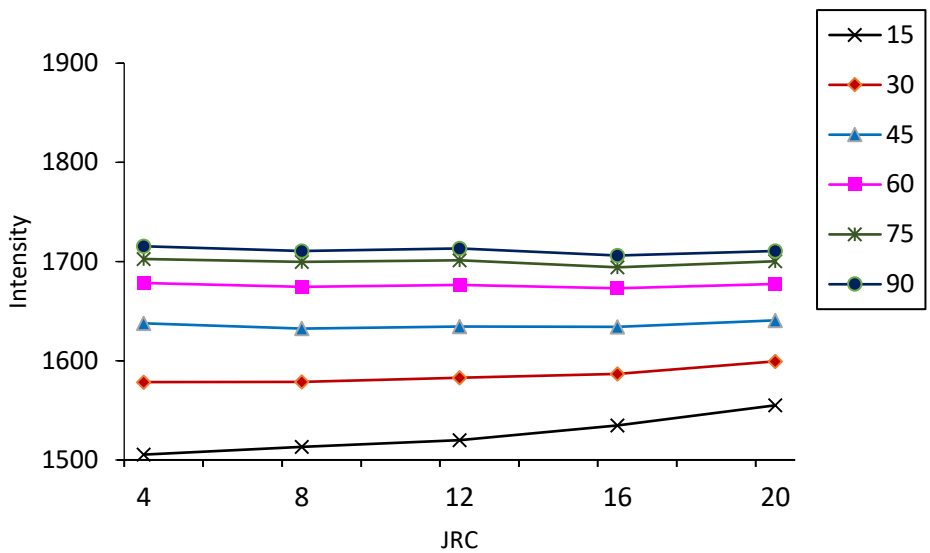

Figure 4.3 Relationship between JRC and intensity at a scanning distance of 5 m. Each line represents a different dip angle

4.1.4 Micro-roughness

Micro-roughness was also considered to be one of the factors that could affect the intensity. Sandpapers of 40, 100, and 220 in grit size were prepared. The sandpapers and the diastones polished with the sandpaper were scanned using LiDAR.

As in the previous experiments, from 5 m to 20 m were spaced at 5 m intervals, and the incidence angle was 0˚ to 75˚ at 15˚ intervals. The results are as follows.

Figure 4.4 represents the intensity measured at a distance of 20 m and the points on each line demonstrate the same dip angle. A graph of a similar shape was drawn for all the distances tested. The smaller the grit number, which means the surface is rougher, the smaller the overall intensity. This is because the rougher the surface, the more the diffusion of the reflection, which leads to smaller intensity.

However, in all the samples, the results were considered to be negligible, considering that the measurements were within 80 which is 4% out of full scale of 2048.

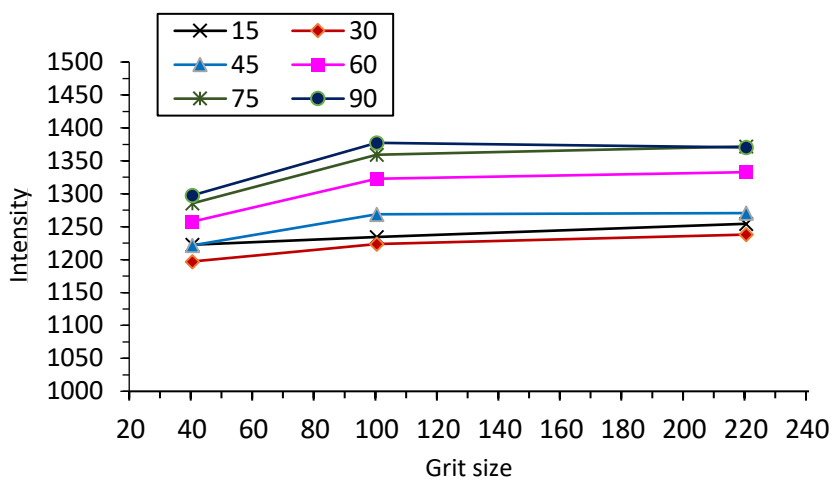

Figure 4.4 Relationship between sandpaper grit size and sandpaper's LiDAR intensity at 20 m scan distance

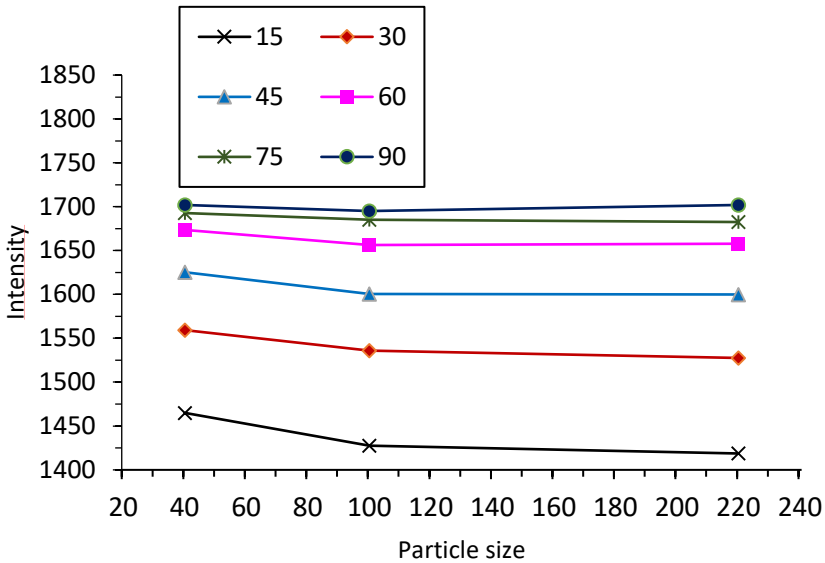

Figure 4.5 Relationship between diastone polished by sandpaper and LiDAR intensity

The results for the diastone samples were different from those of the sandpaper. Given that the surfaces of these samples were rougher as they were rubbed with coarse sandpaper, it was thought that the amount of diffuse reflection and intensity would be smaller but the opposite was confirmed. It was speculated that this resulted from the fact that the surface rubbed with 40 grit size sandpapers was not polished evenly over the entire surface due to the large-sized particles, and, thus, was not representative.

However, considering that there was almost no change in most cases and a difference of approximately 50 in the intensity in the case of an incidence angle of 75, it can be concluded that micro-roughness is not a key factor affecting intensity.

4.1.5 Degree of saturation

Experiments were conducted to investigate the relationship between saturation and intensity. To use rock specimens with different levels of saturation, dry samples, saturated samples, dry samples with their surfaces sprayed, and saturated samples with their surfaces sprayed were used.

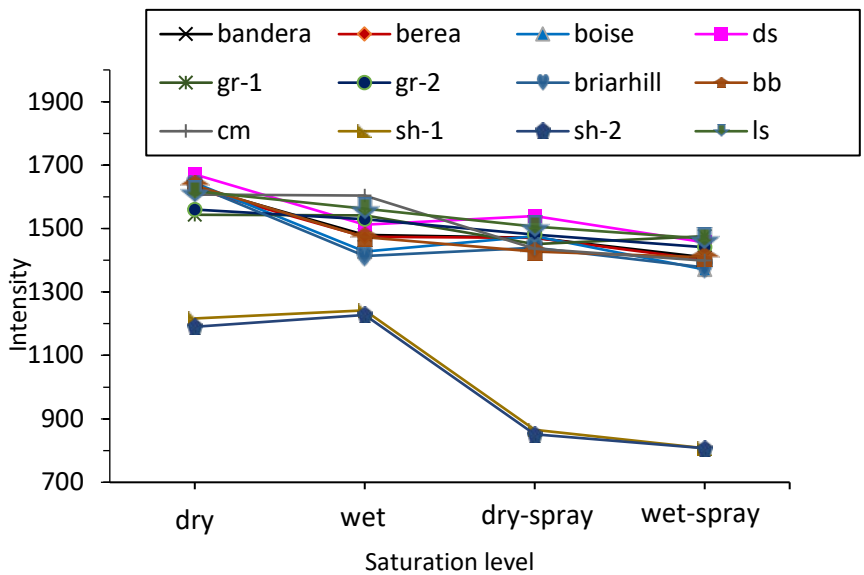

Figure 4.6 Relationship between saturation level and LiDAR intensity at a scan distance of 5 m and incidence angle of 60˚

The samples with high porosity, such as diastone or sandstone, showed large differences between the dry and saturated samples in the intensity readings. As these samples have a high level of porosity, the intensity seems to be determined by the degree of internal saturation rather than the surface characteristics. In contrast, in the case of shale or granite, the difference between the dry sample and the saturated sample was not large, while the difference in the intensity of the sample sprayed with water and the sample not sprayed was large. This shows that, in the case of a sample with low porosity, the difference in saturation inside the rock is not large, therefore,

it is greatly affected by the surface properties.

Franceschi et al. (2009) demonstrated the quantitative relationship between the level of rock saturation and LiDAR intensity. Two type of rocks were tested: marls and limestone. In general, as water content increased by 1%, the intensity decreased by 10% except for a few outliers. Normally, the porosity of limestone is around 10% and that of clay is 55%.

4.1.6 Mechanical and physical properties

In this study, the relationship between the mechanical and physical properties and intensity was also examined. The measured mechanical properties included UCS, specific gravity, porosity, and seismic velocity. The relationship observed between UCS and intensity was as follows. As a result of correcting the effect of the RGB value on the intensity, the relationship between UCS and intensity was linearly proportional. Similar to the UCS, the S-wave and P-wave velocity were in proportion to the intensity.

Ercoli et al. (2013) revealed a linear relationship between the Schmidt hammer rebound value and intensity. In their paper, the Schmidt hammer rebound value and LiDAR intensity had a linear relationship with a slope of 1 at a higher rebound value and 0.5 at a smaller rebound value.

LiDAR intensity and mechanical properties such as UCS and seismic velocity has linear relationship as shown in Figure 4.7.

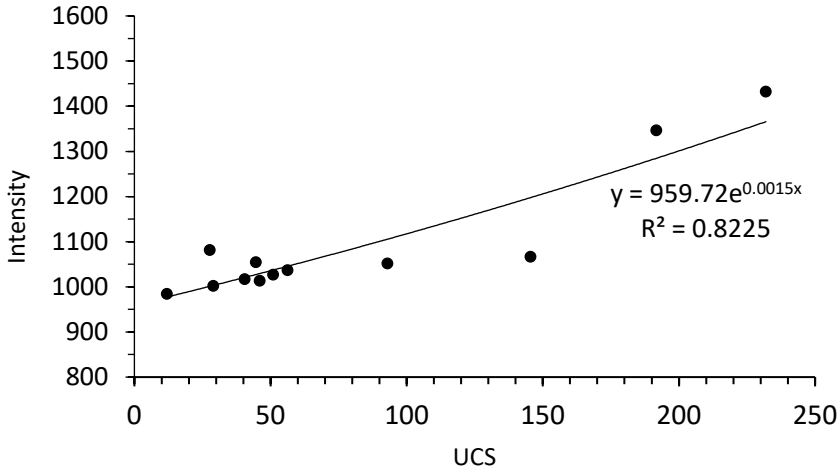

(a)

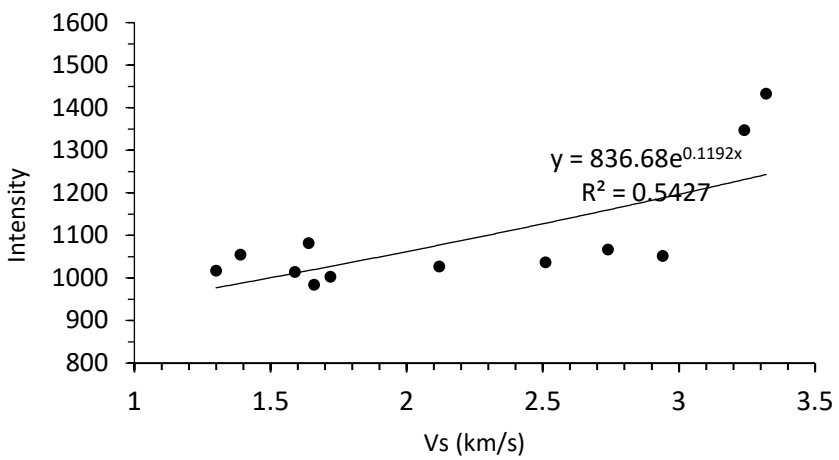

(b)

Figure 4.7 Relationship between LiDAR intensity and mechanical properties (a) UCS, (b)V_S, (c) V_P of wet rock specimens at 5 m and 60˚

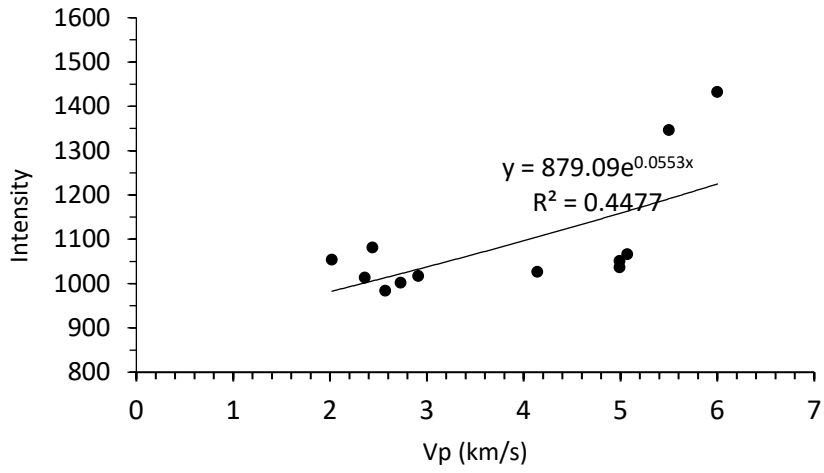

(c)

Figure 4.7. Relationship between LiDAR intensity and mechanical properties (a) UCS, (b)V_P, (c) V_S of wet rock specimens at 5 m and 60˚ (Continued)

In the case of the dry samples, there was no significant difference in intensity depending on the porosity. In the case of the saturated samples, the intensity decreased with increasing porosity. As the porosity increased, the intensity of the wet samples decreased significantly compared to the dry samples. Therefore, it can be noted that as the porosity increased, the intensity difference between the dry sample and the wet sample increased. However, in the case of shale, granite, and limestone samples, whose porosity was close to 0, the value was considered to be an outlier that had no significant relationship to the porosity.

Figure 4.8 describes relationship between porosity and intensity. Figure 4.9 describes relationship between specific gravity and intensity.

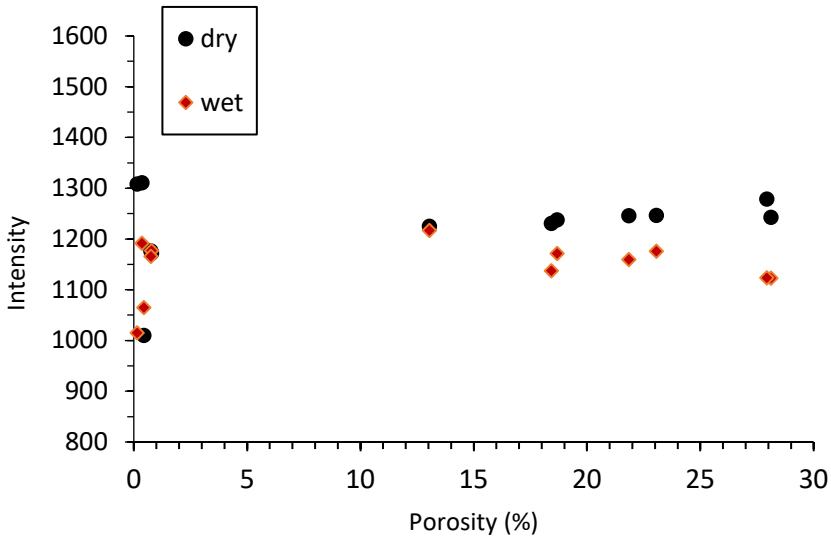

(a)

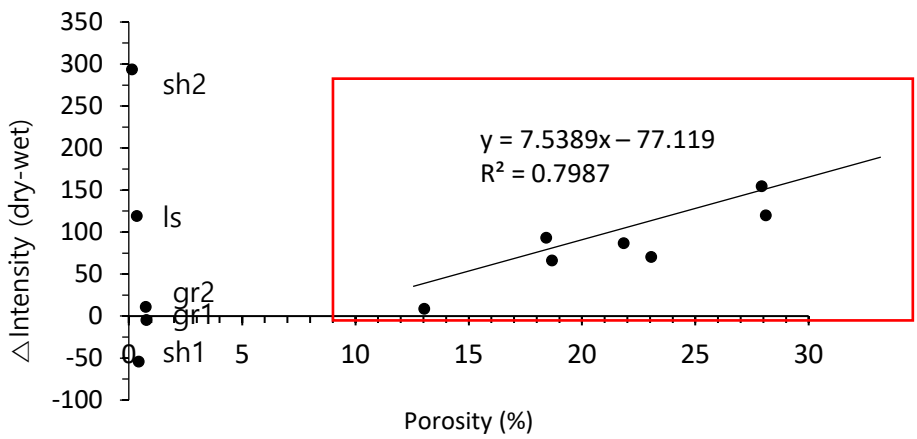

(b)

Figure 4.8 Relationship of porosity and intensity (a) intensity of dry, wet specimen at 5 m and 90˚, (b) intensity difference of dry and wet specimen

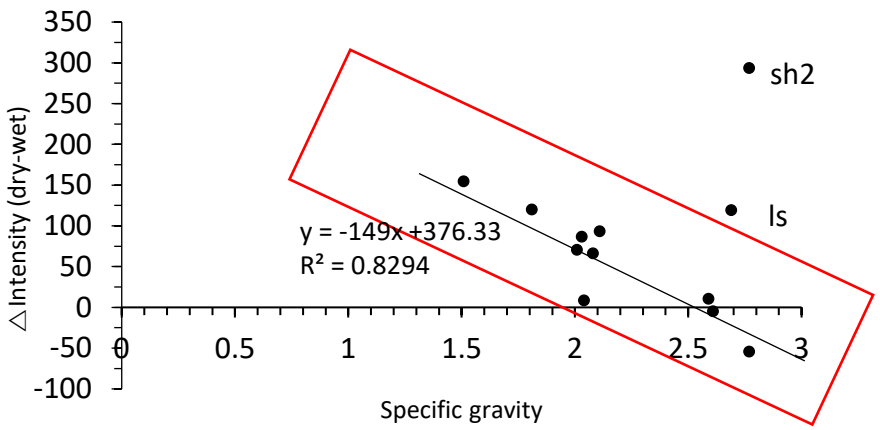

Figure 4.9 Relationship of specific gravity and intensity

4.1.7 Mineral composition

The minerals that make up the rock also affect LiDAR intensity (Burton et al., 2011). The reflectance of a granular surface is complexly controlled by the composition of the individual grains, their weight fractions, and grain sizes. When the photons emitted from the LiDAR laser source encounter the granular surface of an outcrop, some are absorbed while others are scattered. Bright grains (e.g., quartz) scatter the most photons, while dark surfaces (e.g., coal) absorb the majority of the photons. Theoretically, sandstone containing a high percentage of quartz should be more reflective than shale.

A dense rock with a porosity close to 0, such as granite, displays the effect of the RGB value of the surface to intensity well. When the line was extracted close to the diameter of the specimen and the values of the grayscale level, which will be explained in 4.1.8, and intensity according to the position coordinate change were extracted, the Pearson correlation coefficient was 0.843. However, in the case of the

Bandera sandstone, whose porosity is 23.06%, the Pearson correlation coefficient between the grayscale level and intensity was only 0.307. In addition, in the case of a rock in which the approximate mineral composition is known, the approximate location of the corresponding mineral can be determined according to the intensity consistent with the coordinate change.

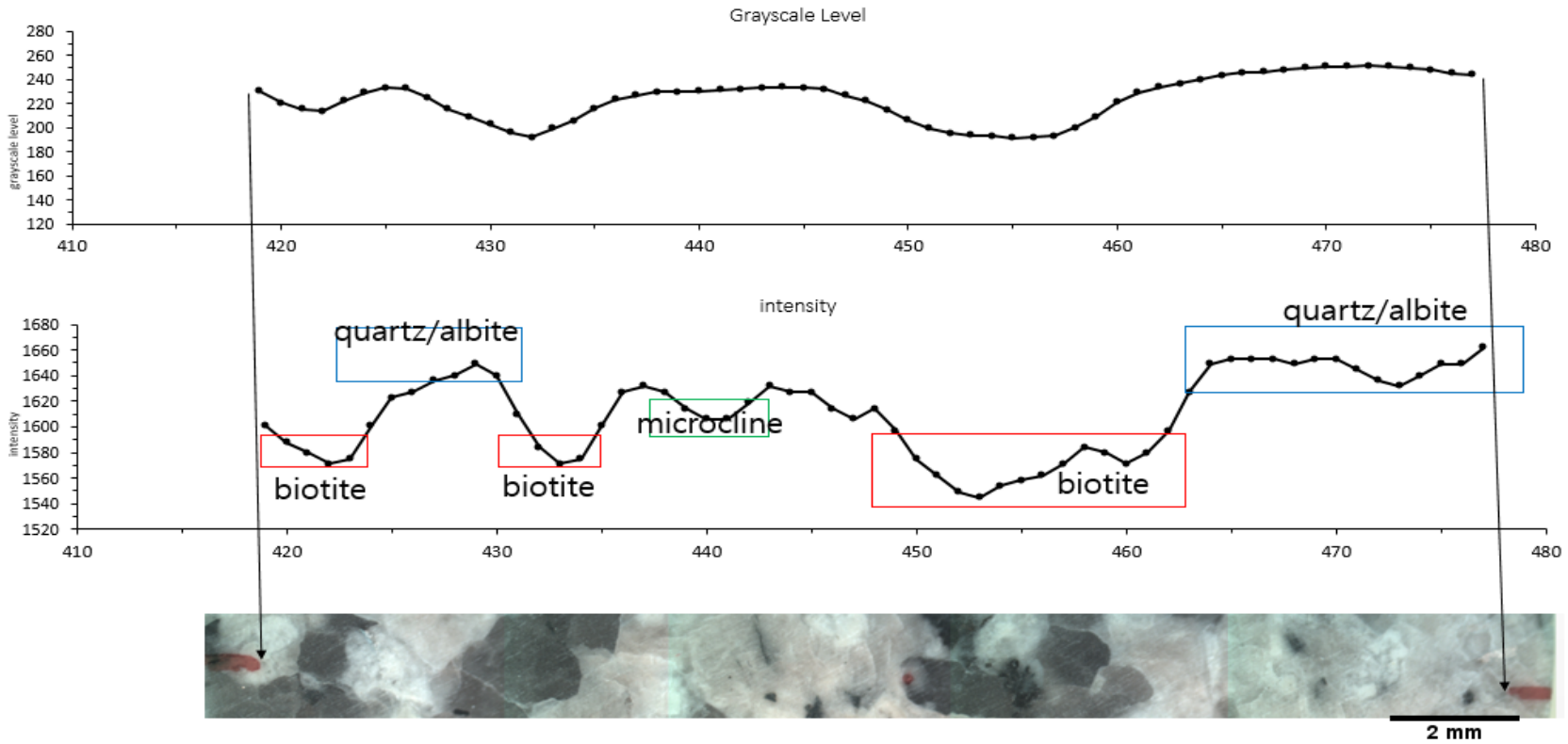

Figure 4.10 Grayscale level, LiDAR intensity, and microscopic picture

It can be seen from Figure 4.10 that the correlation between the grayscale level and intensity was high for granite. Generally, the intensity increases at a high grayscale level and decreases at a low grayscale level. The granite used in the experiment is presumed to be Korean Jeollabukdo Hwangdeung granite. Its constituent minerals are quartz, albite, microcline, and biotite (Wicaksana, 2020). It can be estimated, when comparing the grayscale level with a picture viewed under a microscope, that the constituent mineral of the areas with the highest intensity is quartz or albite, the constituent mineral of the areas with the lowest intensity is biotite, and the constituent mineral of the intermediate region is microcline.

Through this, if the mineral composition of Hwangdeung granite is known, the overall intensity can be estimated. The estimated mineral composition of the granite used in the test and the average LiDAR intensity obtained from it are as follows.

Table 4.1. Average LiDAR intensity from mineral composition

Mineral composition	Weight percent	Average LiDAR intensity
Quartz	35.4	1647
Albite	34.9	
Microcline	20.8	1608
Biotite	8.9	1565
	100	1631.59

The average LiDAR intensity obtained by multiplying the average LiDAR intensity by the weight percentage was 1631.59. The average LiDAR intensity of the whole area of this granite specimen was 1611.98. As a result, it is considered that the average intensity can be reasonably predicted through the mineral composition ratio.

4.1.8 RGB value

Yoo et al. (2015) changed the sum of the RGB value for achromatic color, whose red, green, and blue values are all the same. It influences intensity, and can be defined as a constant linear equation. A correction equation was proposed considering the effect of the RGB values. The corrected reflectance was found to be closely related to the weathering degree of the rock, and it was concluded that it could be used as a more direct indicator of the degree of weathering of the rock

compared to the original reflectance.

It was considered that the simple summation of the RGB values did not properly represent the values of red, green, and blue, hence, the grayscale level, which is the National Television System Committee standard, was used. The red, green, and blue values were multiplied by weights of 0.2989, 0.587, and 0.114, respectively, and then added to obtain a grayscale level. It has been determined that the human eye is the most sensitive to first green, then red, and then blue.

After scanning the RGB table in Figure 3.6 with LiDAR and comparing the intensity of each RGB value, Figure 4.11 was drawn.

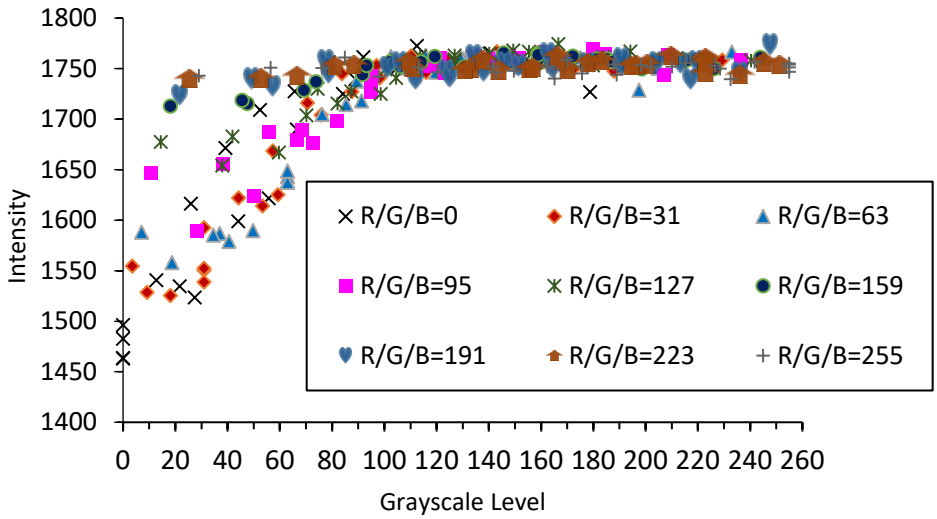

Figure 4.11 Relationship between grayscale level and intensity

This is the sum of the graphs drawn from the column in Figure 3.6. When one of the RGB values was 0, this meant a dark case, and the intensity change according to the grayscale level change was obvious. However, the intensity change according to the grayscale level was insignificant as the value approached 255.

The Kolmogorov-Smirnov (K-S test) was performed to ascertain whether the relationship between the grayscale level and intensity was close to the exponential or polynomial function. The K-S test returns a result for the null hypothesis that the data in vectors x1 and x2 are extracted from the same continuous distribution. The alternative hypothesis is that x1 and x2 are extracted from different continuous distributions. The test rejects the null hypothesis at the 5% significance level.

As a result of performing a K-S test on the value of the cubic function considering the exponential function, logarithmic function, cubic function, and inflection point, it was found that the exponential function was the only case in which the two distributors were not significantly different. The result is shown in Figure 4.12. However, when one of the RGB values was 0, it fitted best with the line

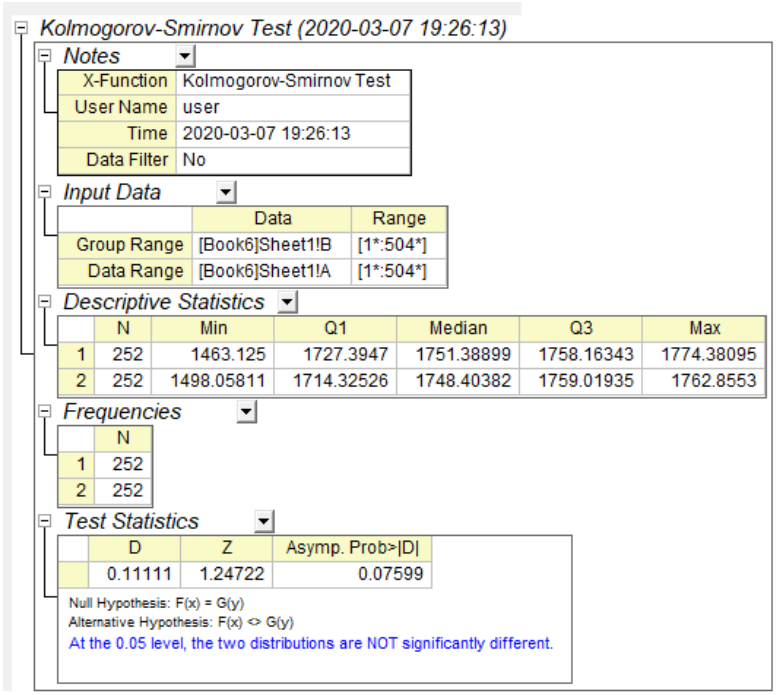

Figure 4.12 Kolmogorov-Smirnov test result for exponential function

representing the whole.

Therefore, the relationship between the grayscale level and LiDAR intensity is presented in Equation 4.1 below.

$$y = 1763.72 - 265.66 * \exp(-0.0225x) \qquad (4.1)$$

However, as can be seen in Figure 4.11, the direct relationship between the grayscale level and intensity is only apparent for the grayscale levels between 0 and 100. Therefore, it would be more accurate to use Equation 4.2, which can be used from grayscale level 0 to 100 after making all grayscale levels of the scanned area linearly less than 100.

$$y = 1840.33 - 323.05 * \exp(-0.0125x) \qquad (4.2)$$

In order to actually correct the RGB values, the RGB values of all the point groups were converted to grayscale levels, and the intensity values at the grayscale levels of the corresponding points were subtracted from the intensity values of the grayscale level of 0, that is, the minimum intensity. The intensity values that differed due to the RGB values were 265.66 when using Equation 4.1 and 323.05 when using Equation 4.2.

4.1.9 Separation

When classifying rock mass, it is important to obtain information about the joints as much as estimating the degree of weathering of the intact rock. This is because most rock masses are discontinuous. In this case, the cement mortar and granite specimens in Figure 3.7 were used.

In all cases, the intensity was checked by exporting the data line as shown in Figure 4.13. The data from the point clouds corresponding to the yellow line in the middle were exported to FARO SCENE program.

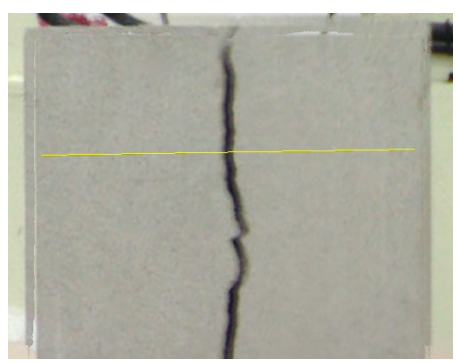

Figure 4.13 Line exported in the FARO Scene program.

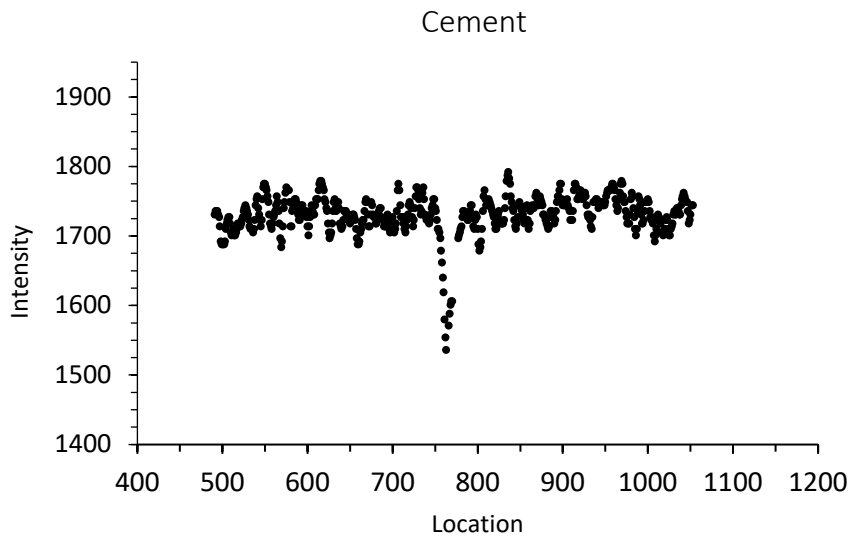

(a)

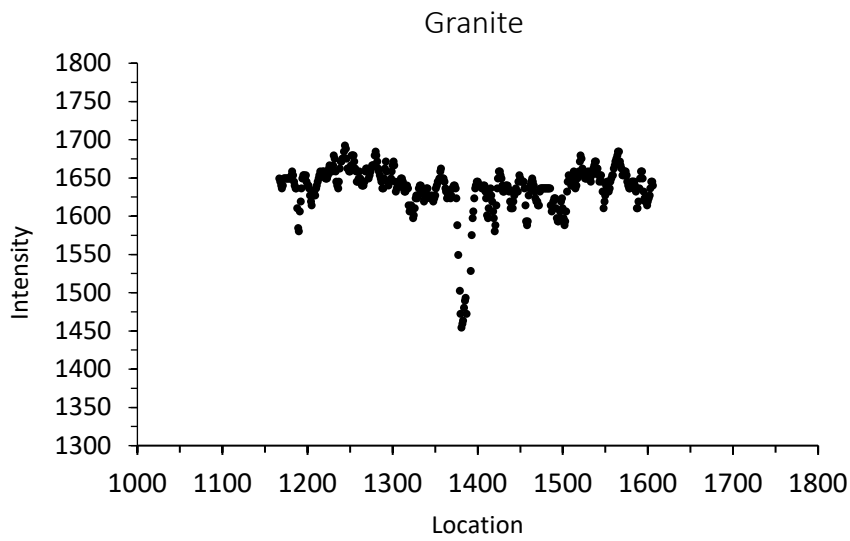

(b)

Figure 4.14 Change of intensity in rock with 6 mm separation

When a separation is present, there is a section in which the intensity is significantly lower than that of the surrounding rock. Since the intensity also decreases when there is infilling material, whether the separation is empty or not should be checked by examining the level of the reduction.

In the FARO S350 equipment used in the experiment, the absolute coordinates of each point are recorded; in this way, the width of the portion where the intensity decreases can be calculated. When used on a wide rock reflection surface rather than in a laboratory experiment, similarly, the ratio of the gap in the entire area can be established by using the intensity of the area where the intensity rapidly decreases in the exported line.

To confirm the accuracy of the intensity for determining separation, the exact separation for each experiment case of cement from 1 mm to 6 mm was checked, which is shown in Table 4.2. As the intensity starts to decrease near the separation, the distance between the decrease in the graph with regard to the average and standard deviation of the rock specimen was checked.

As LiDAR intensity has been shown to be influenced by the edge effect, which means the data changes according to the location, I checked whether the intensity was different as a result of being located in the upper, center, or lower part of the specimen. There was no significant difference between the locations.

Using the LiDAR intensity data, observing 1 mm of separation was not possible. As the ranging error of FARO S350 is ±1mm, this would have been rather difficult. To ascertain separation of less than 1 mm, using point coordinate data would be more suitable than LiDAR intensity data. When using intensity data, further studies on employing a more precise approach need to be conducted.

Table 4.2. Comparing real separation and separation calculated from LiDAR intensity

Separation (mm)	Rock specimen average intensity	Separation calculated from LiDAR intensity (mm)
1	1553.04	x
2	1554.28	3.44
3	1550.36	8.78
4	1551.09	17.22
5	1553.61	21.50
6	1553.44	27.36

4.1.10 Filling material

The typical fillings of rock mass are sand and clay. The results of the scans with dry sand, dry bentonite, wet sand, and wet bentonite in the plastic container are as follows. After obtaining the average intensity for each case, it was corrected based upon a scanning distance of 15 m and an incidence angle of 0˚. The RGB values were also corrected.

Table 4.3. Raw and normalized intensity depending on type of filling

	Raw intensity	Normalized intensity
Dry sand	1626.289	1936.323
Dry bentonite	1673.534	1964.947
Wet sand	1269.996	1632.734
Wet bentonite	1318.543	1672.47

The cement and granite samples depicted in Figure 3.7 were also used to determine the separation. The gaps of each sample were filled with sand and clay of 1 mm and 5 mm, and the change in intensity was examined.

In calculating the joint alteration factor, the effect of the filling's access to water has an influence. Accordingly, the fillings were divided into four types: dry sand, wet sand, dry bentonite, and wet bentonite. As in Figure 4.13, the intensity was checked by exporting the data line by line. After exporting, the effects of the RGB values were normalized. As distinguishing between the separation and the wet infilling material is difficult, the RGB data can be used to differentiate these. The results were as follows.

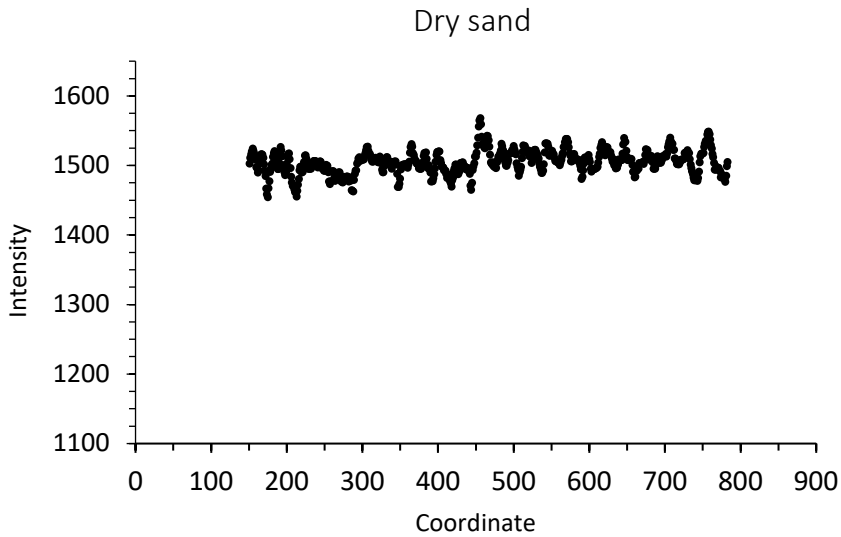

(a)

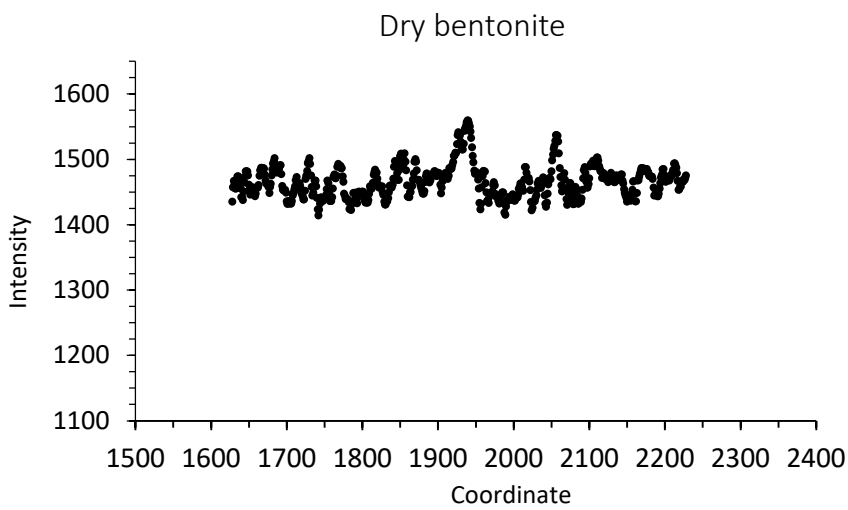

(b)

Figure 4.15 Test results of cement specimen with filling

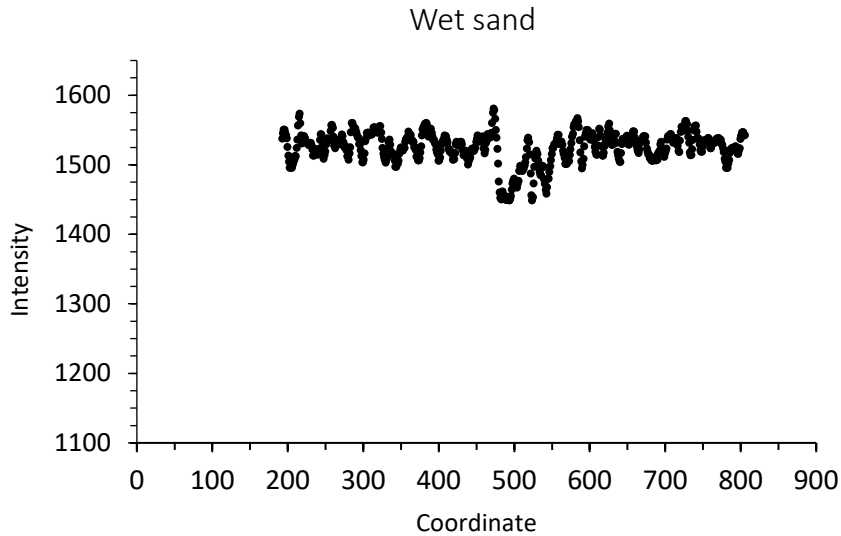

(c)

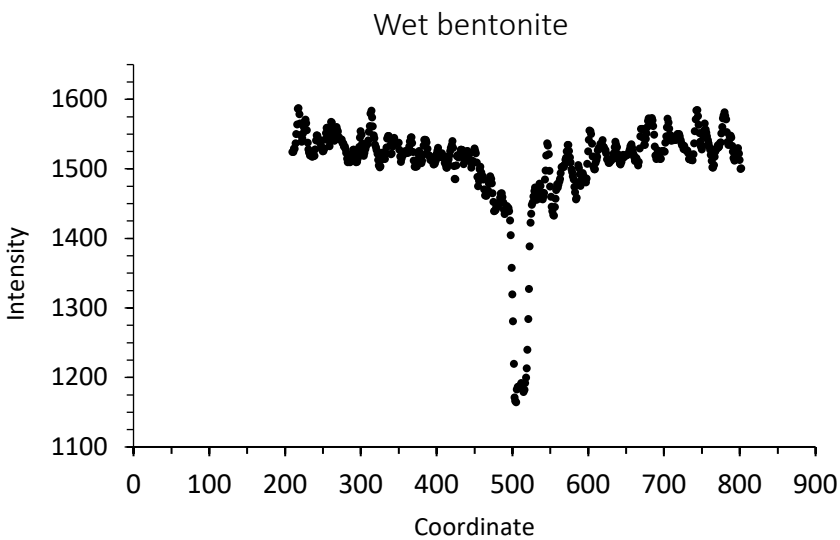

(d)

Figure 4.15 Test results of cement specimen with filling (Continued)

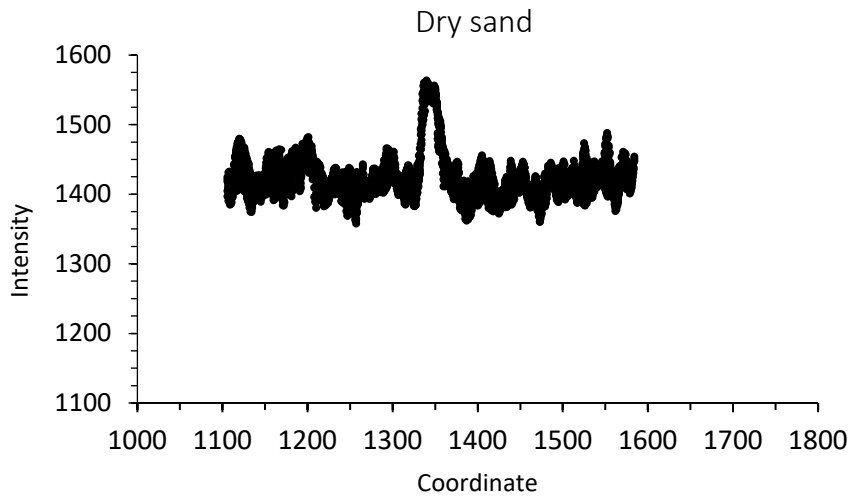

(a)

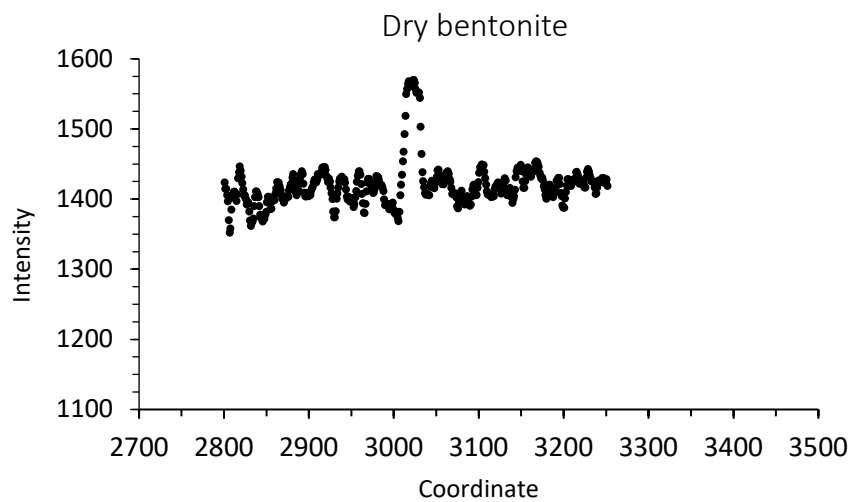

(b)

Figure 4.16 Test results of granite specimen with filling

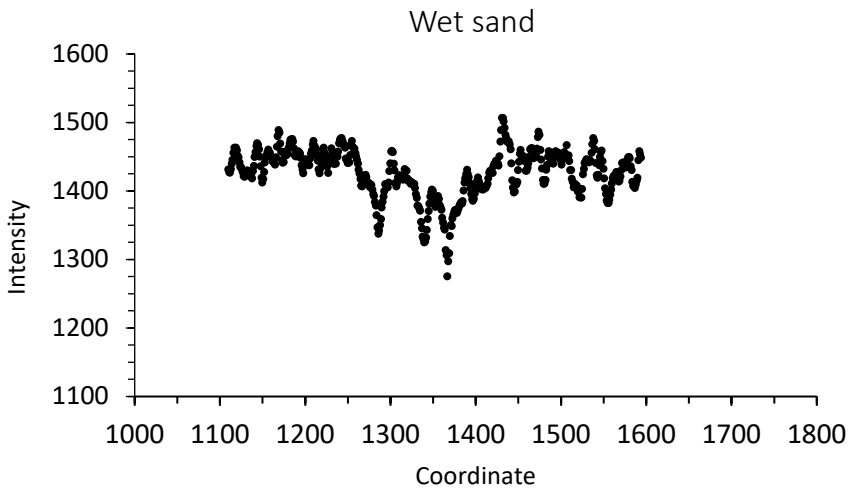

(c)

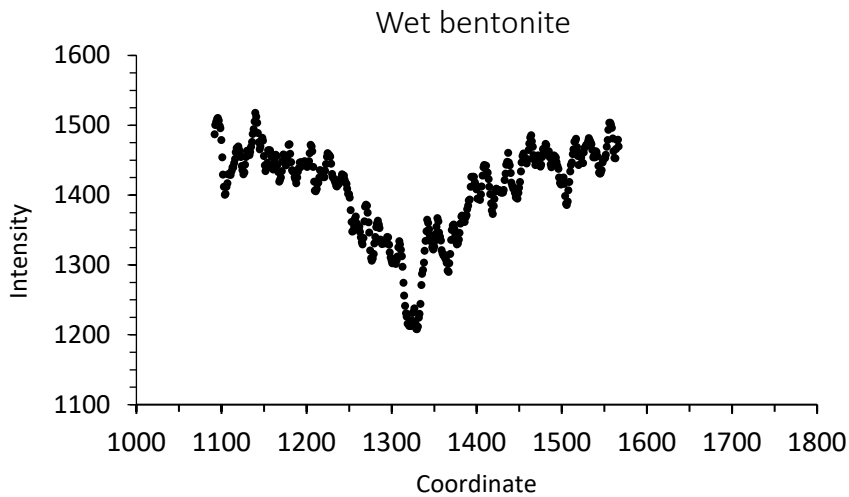

(d)

Figure 4.16 Test results of granite specimen with filling (Continued)

Cement mortar has a similar intensity to sand and bentonite compared to granite, therefore, the difference in the case of the dry filling was not obvious. However, in all cases, the intensity of the area with the filling was different.

Table 4.4. Change of intensity in filling area (a) cement mortar specimen, (b) granite specimen

(a)

	Cement mortar average intensity	Peak filling intensity	%
Separation	1464.934	1367.834	-6.63
Dry sand	1420.729	1552.811	+9.3
Dry bentonite	1414.003	1569.439	+10.99
Wet sand	1435.849	1299.656	-9.49
Wet bentonite	1448.944	1175.404	-18.88

(b)

	Granite average intensity	Peak filling intensity	%
Separation	1551.461	1391.481	-10.31
Dry sand	1503.562	1567.881	+4.28
Dry bentonite	1462.168	1559.59	+6.66
Wet sand	1530.266	1448.469	-5.35
Wet bentonite	1528.066	1164.015	-23.82

The rate of the change in LiDAR intensity varies depending on the type of filling. In both the granite and cement mortar cases, the intensity change was greater when the bentonite was used as the filling rather than the sand filling. Specifically, the intensity increased when the aperture was filled with sand and decreased when the aperture was filled with bentonite. The precise figures are shown in Table 4.4.

However, while placing the wet infilling material inside the aperture, water may also have made the periphery side wet, which might have influenced the change in the intensity slightly.

4.1.11 Summary

Each factor differed in terms of the amount of importance it had in affecting LiDAR intensity. To summarize this, Figure 4.17 illustrates the degree to which each factor influenced intensity.

The RGB value converted to the grayscale level had the most influence, followed by the incidence angle, and distance. The intensity will also vary depending upon the material. For example, fresh snow gives a very high intensity reading, while dark soil does very low. However, since all the samples used in the experiment were rocks, they did not exhibit intensity across the entire range from 0 to 2047. The laboratory experiment results showed that the intensity was distributed between approximately 700 and 1700. The influence of each factor within the interval is as shown in Figure 4.17. The maximum and minimum values used are the averaged values. Table 4.5 shows impact of each factors to the LiDAR intensity.

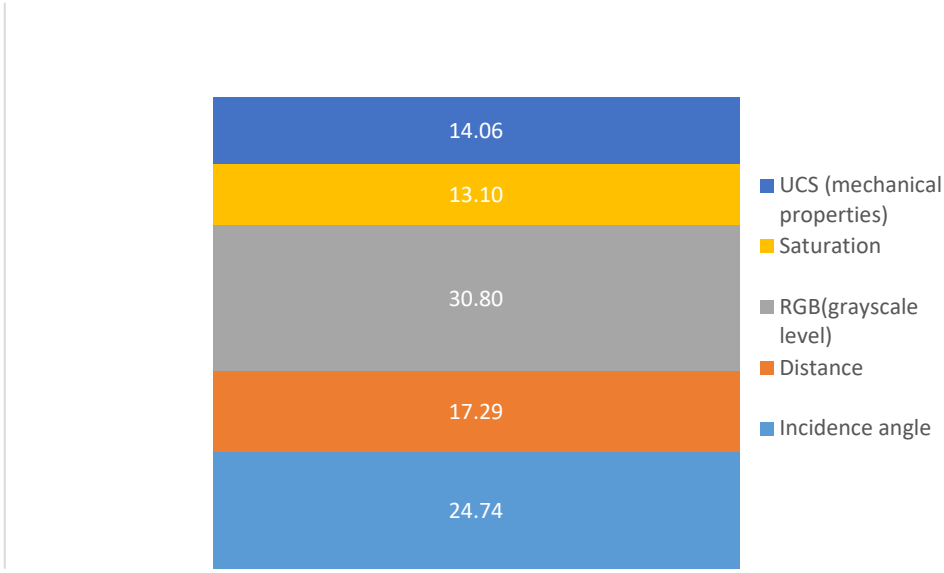

Figure 4.17 Degree of factors affecting LiDAR intensity

Table 4.5. Degree of influence of each factor upon LiDAR intensity

	Maximum-minimum	%
Incidence angle	250	24.74
Distance	174.72	17.29
RGB (grayscale level)	311.26	30.80
Saturation	132.41	13.10
UCS (mechanical properties)	142.11	14.06
Sum	1010	100

4.2 Application of LiDAR intensity to determination of the joint alteration factor determination

4.2.1 GSI joint alteration factor

Ultimately, the purpose of this paper was to find the joint alteration factor of GSI through LiDAR intensity. Yoo et al. (2015) and Fowler et al. (2011) showed that the LiDAR intensity was a sufficient value to represent the state of the overall rock mass. Therefore, it was estimated that a rock mass exhibiting generally large intensity measurements would have a large joint alteration factor.

Among the factors affecting intensity, the incidence angle, distance, and RGB were considered to be factors that have a large effect and are independent of the joint alteration factors. For this reason, the effects of those factors were corrected.

4.2.2 Field applications

Three sites of rock slope were selected to examine the applicability of the joint alteration factor determination to real rock cases. Two of the rock slopes are located at Bangudae Petroglyphs located in Ulsan, Ulju-gun, Eonyang-eup, Daegok-ri, 991. The other rock slope is in Gwanaksan Park near Seoul National University, College of Engineering in Daehak-dong, Gwanak-gu, Seoul.

(a)

Figure 4.18 Panorama picture of task section (a) site 1, (b) site 2, 3

(b)

Figure 4.18 Panoramic picture of task section (a) Site 1, (b) Sites 2 and 3 (Continued)

RMR and J_a of each site have been hand mapped. Table 4.6 shows the location and physical properties of the rock slopes.

Table 4.6. Location and rock mass classes of task section

No	Location (GPS)	UCS (MPa)	RMR-discontinuities condition	RMR class	J_a
1	Gwanaksan (37.453953, 126.948964)	233.7	21-28	II	0.75-2
2	Bangudae Petroglyphs (35.603984, 129.177561)	49.6	17	III	1-3
3	Bangudae Petroglyphs fractured zone (35.603984, 129.177561)	42.5	8	IV	2-4

The results of correction with respect to the distance, incidence angle, and RGB values by acquiring the LiDAR data at each site are presented in Table 4.7. Each site was adjusted to have 330,000-360,000 points.

Table 4.7. RMR rating at (a) site 1, (b) site 2, (c) site 3

(a)

Rating item	Measurement	Rating
UCS (MPa)	233.7	12
RQD (%)	36.25	8
Spacing of discontinuity (m)	0.2 - 0.6	10
Persistence (m)	1 - 3	4
Separation (mm)	1.7	1 - 4
Roughness	Average JRC 10.56 (Slightly rough)	3
Infillings (mm)	None	6
Weathering	Slightly weathered - Unweathered	5 - 6
Ground water condition (litres/min)	None	15
Basic RMR		64 - 68

(b)

Rating item	Measurement	Rating
UCS (MPa)	45	5
RQD (%)	46	9
Spacing of discontinuity (m)	0.8	6
Persistence (m)	<1	6

Separation (mm)	1 - 5	1
Roughness	Smooth	1
Infillings (mm)	None	6
Weathering	Moderately weathered	3
Ground water condition (litres/min)	<10	10
Basic RMR		47

(c)

Rating item	Measurement	Rating
UCS (MPa)	43	5
RQD (%)	32	7
Spacing of discontinuity (m)	0.1	7
Persistence (m)	>20	0
Separation (mm)	>5	0
Roughness	Slightly rough	3
Infillings (mm)	Soft filling, <5	2
Weathering	Moderately weathered	3
Ground water condition (litres/min)	<10	10
Basic RMR		37

For Site 1, which is in Gwanaksan, the UCS was measured from the Schmidt rebound value. A point load test was also conducted in the laboratory. The UCS

calculated from the point load test was 190.4 MPa, which did not change the RMR result.

Table 4.8. Correcting scanning distance effect

No	Raw intensity	Scanning distance (m)	Scanning distance correction value
1	1567	10	+44.2
2	1330	32	+136.26
3	1258	27	+120.73

For the distance correction, the reference distance was set to 15 m. Though 15 m was concluded to be the ideal distance for scanning in Chapter 4.1.1, it was impossible to place the LiDAR at a 15 m distance from three of the rock masses upward as there was a stream and cliff that prevented this.

In addition to the distance, the RGB and incidence angle were corrected for each location.

Table 4.9. Correcting incidence angle effect

No	Raw intensity	Average incidence angle (˚)	Incidence angle correction value
1	1567	35.43	+98.42
2	1330	26.65	+74.04
3	1258	10.51	+29.2

To perform an accurate correction, considering the plane and dip angle to calculate the incidence angle for every different point cloud would be the ideal. However, LiDAR with high resolution has many point clouds. The FARO S350 has a resolution of 1 mm, which means it has approximately 100,000 points in a 1 m x 1 m area. Constituting the planes and calculating the attitude of each plane would take

considerable time and energy, hence, using the overall dip angle of the rock mass for correcting was assumed to be sufficient. The average rock slope attitude was calculated from the xyz coordinates obtained from LiDAR.

FARO BuildIT software was used to complete this process. The program constructs the plane and calculates the normal vector of each point. The normal vector was exported and used to calculate the incidence angle of every point cloud. The difference in the average of the two methods was approximately 37. The number of points in each corrected intensity range is shown in Figure 4.19. Table 4.10 shows number of points in the range of the corrected intensity.

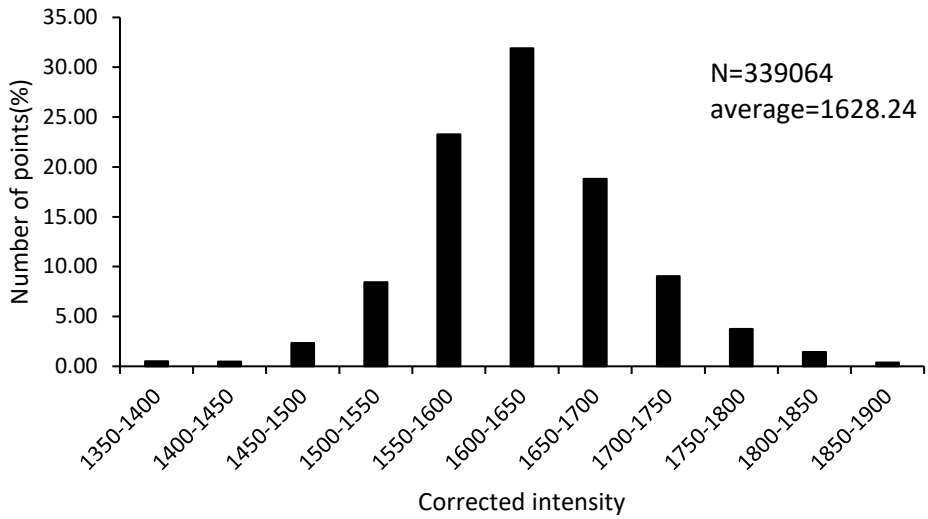

(a)

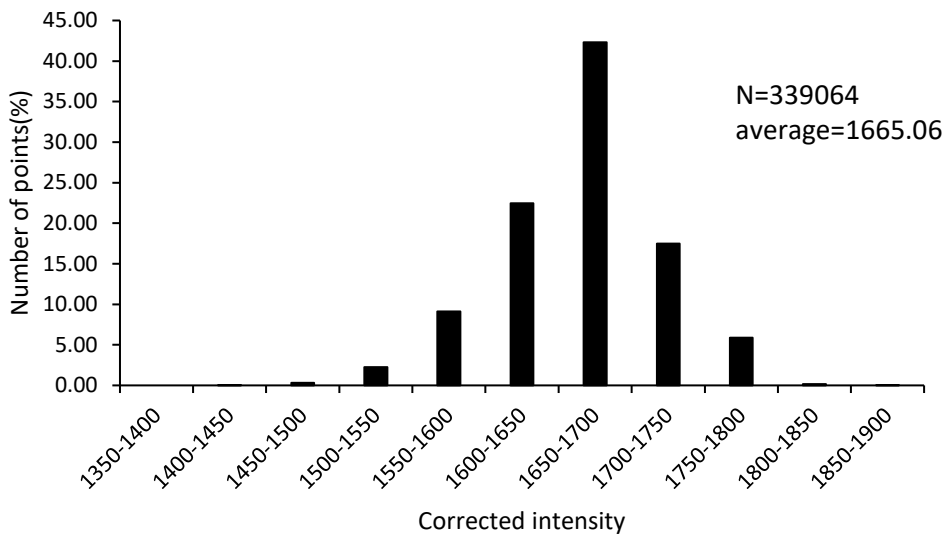

(b)

Figure 4.19 Number of points in each intensity group after correcting the incidence angle (a) considering each point's incidence angle, (b) calculating average dip angle

Table 4.10. Number of points in the range of the corrected intensity

Corrected intensity	Each (number)	Each (%)	Average (number)	Average (%)
1300-1350	2	0.01	0	0.00
1350-1400	171	0.50	0	0.00
1400-1450	1565	0.46	57	0.02
1450-1500	7922	2.34	1108	0.33
1500-1550	28622	8.44	7579	2.24
1550-1600	78908	23.27	30915	9.12
1600-1650	108155	31.90	76121	22.45
1650-1700	63714	18.79	143496	42.32
1700-1750	30674	9.05	59248	17.47
1750-1800	12666	3.74	19926	5.88
1800-1850	4841	1.43	603	0.18
1850-1900	1304	0.38	11	0.00

According to the method that considered the incidence angle of each point, the number of points that belonged to the 1600-1650 range was the highest, and according to the method using the average, the number of points that belonged to the 1650-1700 range was the largest.

Though considering each point's incidence angle is the most accurate method, using the average dip angle to calculate the incidence angle would be adequate for obtaining the joint alteration factor as a difference of approximately 50 out of 2047 can be ignored and the joint alteration factor is calculated as a rough range in this paper.

Table 4.11. Correcting the grayscale level effect

No	Raw intensity	Average grayscale level	Grayscale level correction value
1	1567	167.33	-177.74
2	1330	143.66	-163.3
3	1258	194.05	-198.27

In the case of Site 1, the average correction value of the grayscale level was -177.74. The correction of each point was compared with its own RGB value and the correction with the average RGB value. Although using the points' own RGB values is the most accurate method, using the average RGB is sufficient for convenient correction. Table 4.12 shows the difference between the two correction methods. Number 1 shows the minimum, median, and maximum value of the corrected point clouds using each point's own RGB and Number 2 shows the corrected value using the average RGB of Site 1. The comparison between the numbers of points for the two methods is shown in Figure 4.20 and Table 4.13.

Table 4.12. Comparing the correction of grayscale level effect

No	Min	Median	Max
1	1119.52	1393.33	1589.7
2	1149.26	1390.26	1586.26

Table 4.13. Number of points in the range of corrected intensity

Corrected intensity	Each (number)	Each (%)	Average (number)	Average (%)
1100-1150	35	0.01	1	0.00
1150-1200	535	0.16	405	0.12
1200-1250	4133	1.22	3774	1.11
1250-1300	17507	5.16	14939	4.41
1300-1350	55248	16.29	46940	13.84
1350-1400	109229	32.21	140261	41.37
1400-1450	108990	32.14	91777	27.07
1450-1500	39936	11.78	34340	10.13
1500-1550	3409	1.01	6558	1.93
1550-1600	42	0.01	69	0.02

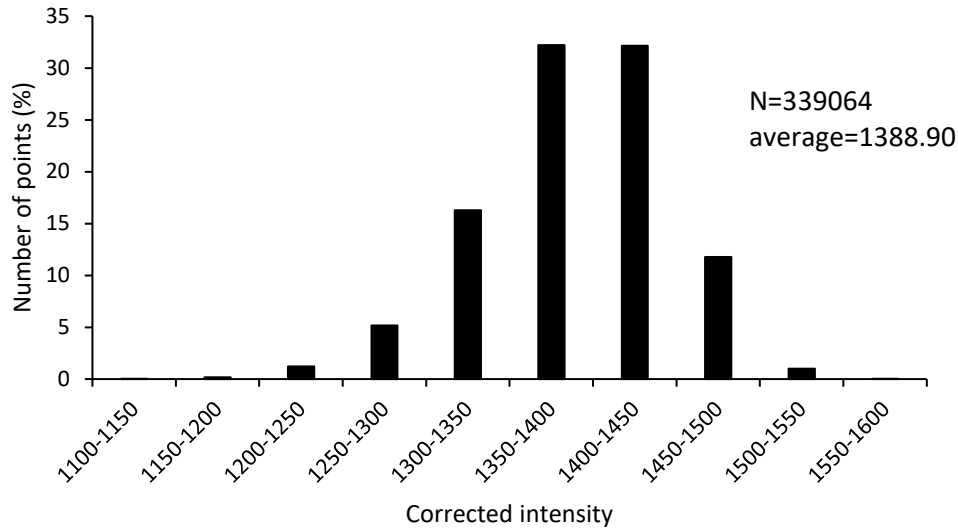

(a)

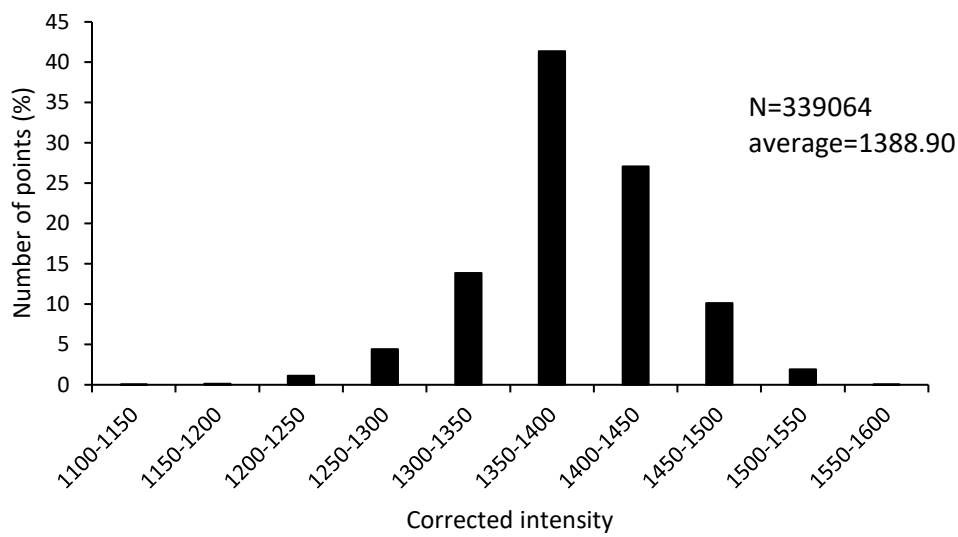

(b)

Figure 4.20 Number of points in each intensity group after correcting RGB value in grayscale (a) considering each point's grayscale level, (b) calculating by average grayscale

Table 4.14 Raw and corrected intensities at three sites of rock slope

Site No.	Raw intensity	Scanning distance correction value	Incidence angle correction value	RGB (Grayscale level) correction value	Corrected intensity	J_a
1	1567	+44.2	+98.42	-177.74	1532	0.75-2
2	1330	+136.26	+74.04	-163.3	1377	1-3
3	1258	+120.73	+29.2	-198.27	1210	2-4

As the intensity of the FARO laser scanner is shown in integers from 0 to 2047, the averaged raw intensity and corrected intensity were rounded off to the nearest integer.

Table 4.13 shows the results of this study. After correcting the distance, incidence angle, and grayscale level, the corrected intensity was shown to be more comparative to the joint alteration factor. Before correction, the difference between Site 2 and 3 was 72, which is a difference of just 3.5%. After correction, the gap between Site 1 and Site 2 was 155, while between Site 2 and Site 3 the gap was 167. Consequently, a rock mass with a corrected intensity similar to that of Site 1 can be regarded as having a joint alteration factor of 0.75-2, as was the case with Sites 2 and 3.

From LiDAR intensity, many factors can be reasonably estimated. When all the other factors are the same, UCS increases as intensity increases. For bigger RMR discontinuities condition, intensity increases. Not only joint alteration factor, but also RMR discontinuities condition and UCS of rock mass can be evaluated roughly from LiDAR intensity data.

Chapter 5. Conclusions

In this study, a series of test in a laboratory scale were performed to investigate the characteristics of LiDAR intensity. Several rock and rock-like specimens were selected with regards to the rock types and mechanical properties. Five different sandstones (Bandera, Berea, Boise, Briarhill, and Buff Berea), two granites, two shales, cement mortar, diastone, and limestone were used. Additionally, to confirm its usefulness and increase its usability, three sites of rock slope were selected to demonstrate the results of the study.

Previous studies have shown that LiDAR intensity is affected by the mineral composition of rock, rock strength, and degree of weathering. The relationships between LiDAR intensity and distance, incidence angle, roughness, degree of saturation, mechanical properties (UCS, V_P, V_S, porosity), mineral composition, and RGB value were analysed. Laboratory experiments were conducted to quantitatively determine to what degree the intensity was influenced by these factors. Specimens of various types of sandstone, granite, shale, limestone, cement, and diastone were made into Brazilian disc and attached to an acrylic plate and then scanned with LiDAR at various distances and angles. In order to investigate the relationship between water saturation and intensity, experiments were conducted on dry specimens, saturated specimens, dry specimens with water on the surface, and saturated specimens with water on the surface. As a result, it was concluded that the scanning distance, incidence angle, saturation condition, mechanical properties, mineral composition, and RGB value of rock are directly related to LiDAR intensity.

In the case of rock, the factors that influenced the LiDAR intensity were RGB (29.36%), incidence angle (23.58%), scanning distance (16.48%), mechanical properties (13.41%), degree of saturation (12.49%), and roughness (4.72%) in the

order of importance. By these factors, the intensity of rock measures from 700 to 1700 when FARO S350 is used that provides an intensity scale between 0 and 2047.

The color value expressed in RGB is the factor that influenced the intensity the most at 29.36%. To obtain the exact relationship, a color palette of various RGB combinations was printed and scanned with LiDAR. The grayscale level calculated by giving a certain weight to each RGB value showed a high correlation with the intensity and could be used for correction. However, it was observed that it is more accurate to convert the full grayscale level to a value of intensity 100 and use that to correct the intensity.

Each factor involved a different method of correction. For the scanning distance, for distances less than 15 m, the average relationship produced through the experiments was used. For distances over 15 m, the relationship whereby the LiDAR intensity was inversely proportional to the square of the distance was used. For the incidence angle, I used a linear equation obtained from the experiments. For RGB (grayscale level) correction, the exponential equation using the K-S test was used.

To investigate the effect of separation and filling, an experiment was conducted using cuboid rock samples. In the case of granite, the intensity change across the separation was -6.7%, + 9.3% for dry sand, + 11% for dry bentonite, -9.5% for wet sand, and -18.9% for wet bentonite. These were the differences after correcting the irrelevant values such as scan distance, incidence angle, and RGB. As the intensity decreases in both the separation and the area with infilling material, the RGB value can be used to detect whether it is separation or infilling material providing the result.

The result of comparing the hand mapping data and the LiDAR intensity for three locations indicated the relationship between intensity and the joint alteration factor. In this regard, for convenience, using the average value for correction would be sufficient. For rock mass with an intensity of approximately 1532 after correction, the joint alteration factor was 0.75-2. In the case of a rock mass with an intensity of

approximately 1337 and 1210, the joint alteration factor of each would be 1-3 and 2-4, respectively. The relationship would be more accurate if the relevant area consists of similar rock types to the studied areas, which was granite at Site 1, and sandstone and clay rock at Site 2 and Site 3. The standard deviation of intensity increases according to the increase in degree of weathering as shown in Appendix A.

Reference

Kim, J., Kwon, K.K. and Lee, S.I., 2012. Trends and Applications on Lidar Sensor Technology, [ETRI] Electronics and Telecommunications trends, 27(6), pp.134-143. (in Korean)

Lee, S. and Jeon, S., 2016. A Study on the Extraction of Slope Surface Orientation using LIDAR with respect to Triangulation Method and Sampling on the Point Cloud. Tunnel and Underground Space, 26(1), pp.46-58. (in Korean)

Lee, S. and Jeon, S., 2017. A Study on the Roughness Measurement for Joints in Rock Mass Using LIDAR. Tunnel and Underground Space, 27(1), pp.58-68. (in Korean)

Shin, J.I., 2007. Signal characteristics analysis and normalization of LiDAR intensity data, Master's Thesis, Inha University. (in Korean)

Yoo, W.K., Kim, J. and Kim, T.H., 2015. The Relationship between Weathering Degree and Reflectance of Laser Scanner Considering RGB Value, Journal of the Korea Academia-Industrial cooperation Society, 16(10), pp.7182-7188. (in Korean)

Abellán, A., Oppikofer, T., Jaboyedoff, M., Rosser, N.J., Lim, M. and Lato, M.J., 2014. Terrestrial laser scanning of rock slope instabilities. Earth Surface Processes and Landforms, 39(1), pp.80-97.

Bellian, J.A., Kerans, C. and Jennette, D.C., 2005. Digital outcrop models: applications of terrestrial scanning lidar technology in stratigraphic modeling. Journal of Sedimentary Research, 75(2), pp.166-176.

Burton, D., Dunlap, D.B., Wood, L.J. and Flaig, P.P., 2011. Lidar intensity as a remote sensor of rock properties. Journal of Sedimentary Research, 81(5), pp.339-347.

Cai, M., Kaiser, P.K., Uno, H., Tasaka, Y. and Minami, M., 2004. Estimation of rock mass deformation modulus and strength of jointed hard rock masses using the GSI system. International Journal of Rock Mechanics and Mining Sciences, 41(1), pp.3-19.

Cai, M., Kaiser, P.K., Tasaka, Y. and Minami, M., 2007. Determination of residual strength parameters of jointed rock masses using the GSI system. International Journal of Rock Mechanics and Mining Sciences, 44(2), pp.247-265.

Coren, F. and Sterzai, P., 2006. Radiometric correction in laser scanning. International Journal of Remote Sensing, 27(15), pp.3097-3104.

Ercoli, L., Megna, B., Nocilla, A. and Zimbardo, M., 2013. Measure of a limestone weathering degree using laser scanner. International Journal of Architectural Heritage, 7(5), pp.591-607.

Fowler, A., France, J.I. and Truong, M., 2011. Applications of advanced laser scanning technology in geology. Riegl USA. http://www. rieglusa. com/pdf/applications-ofadvanced-laser-scanning-technology-in-geology-ananda-fowler-final. pdf. (May. 20. 2020)

Franceschi, M., Teza, G., Preto, N., Pesci, A., Galgaro, A. and Girardi, S., 2009. Discrimination between marls and limestones using intensity data from terrestrial laser scanner. ISPRS Journal of Photogrammetry and Remote Sensing, 64(6), pp.522-528.

Gatziolis, D. and Andersen, H.E., 2008. A guide to LIDAR data acquisition and processing for the forests of the Pacific Northwest. Gen. Tech. Rep. PNW-GTR-768. Portland, OR: US Department of Agriculture, Forest Service, Pacific Northwest Research Station. 32p.

Hoek, E., Marinos, P. and Benissi, M., 1998. Applicability of the Geological Strength Index (GSI) classification for very weak and sheared rock masses. The case of the Athens Schist Formation. Bulletin of Engineering Geology and the Environment, 57(2), pp.151-160.

Junttila, S., Sugano, J., Vastaranta, M., Linnakoski, R., Kaartinen, H., Kukko, A., Holopainen, M., Hyyppä, H. and Hyyppä, J., 2018. Can leaf water content be estimated using multispectral terrestrial laser scanning? A case study with Norway Spruce seedlings. Frontiers in Plant Science, 9, 299.

Kaasalainen, S., Jaakkola, A., Kaasalainen, M., Krooks, A. and Kukko, A., 2011. Analysis of incidence angle and distance effects on terrestrial laser scanner intensity: Search for correction methods. Remote Sensing, 3(10), pp.2207-2221.

Klise, K.A., Weissmann, G.S., McKenna, S.A., Nichols, E.M., Frechette, J.D., Wawrzyniec, T.F. and Tidwell, V.C., 2009. Exploring solute transport and streamline connectivity using lidar-based outcrop images and geostatistical representations of heterogeneity. Water Resources Research, 45(5).

Kukko, A., 2013. Mobile Laser Scanning–System development, performance and applications. Finnish Geodetic Institute.

Memari, A.M., Iulo, L.D., Solnosky, R.L. and Stultz, C.R., 2014. Building integrated photovoltaic systems for single family dwellings: innovation concepts. Open Journal of Civil Engineering, 4.02, 102.

Pesci, A., Teza, G. and Ventura, G., 2008. Remote sensing of volcanic terrains by terrestrial laser scanner: preliminary reflectance and RGB implications for studying Vesuvius crater (Italy). Annals of Geophysics, 51(4), pp.633-653.

Tan, K. and Cheng, X., 2015. Intensity data correction based on incidence angle and distance for terrestrial laser scanner. Journal of Applied Remote Sensing, 9(1), 094094.

Wicaksana, Y., 2020. Prediction of rock cutting performance and abrasiveness considering dynamic properties at intermediate strain rate, Doctoral dissertation, Seoul National University.

Appendix A. LiDAR intensity of point clouds in each site before and after correction

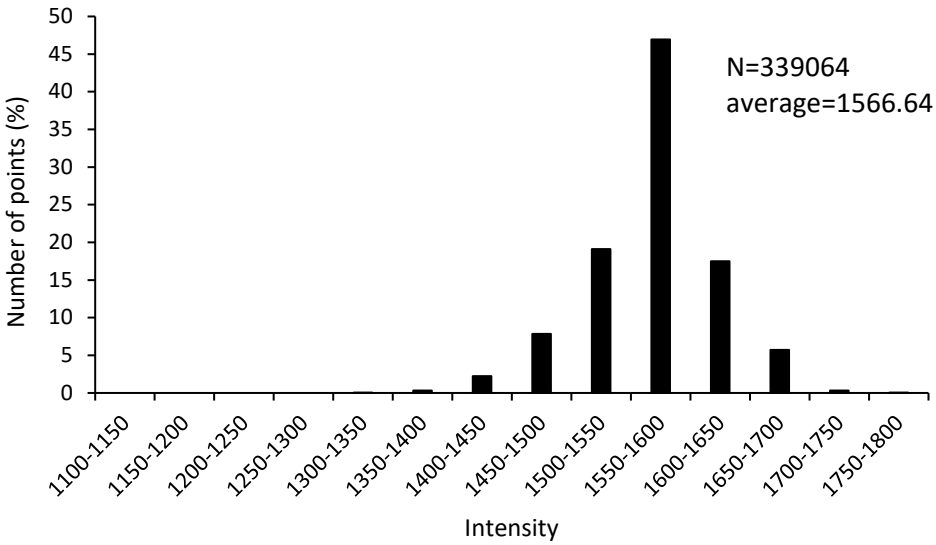

Figure A.1 Raw intensity distribution (Site 1)

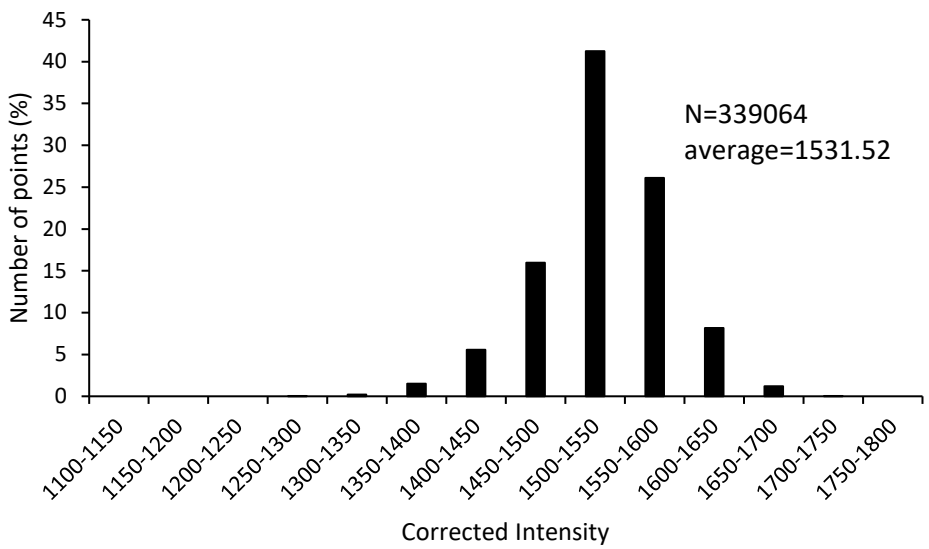

Figure A.2 Corrected intensity distribution (Site 1)

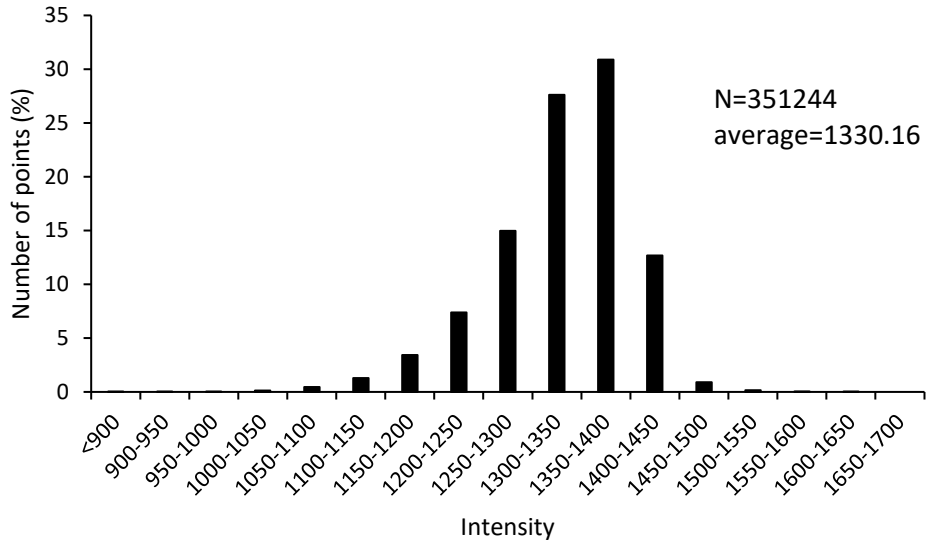

Figure A.3 Raw intensity distribution (Site 2)

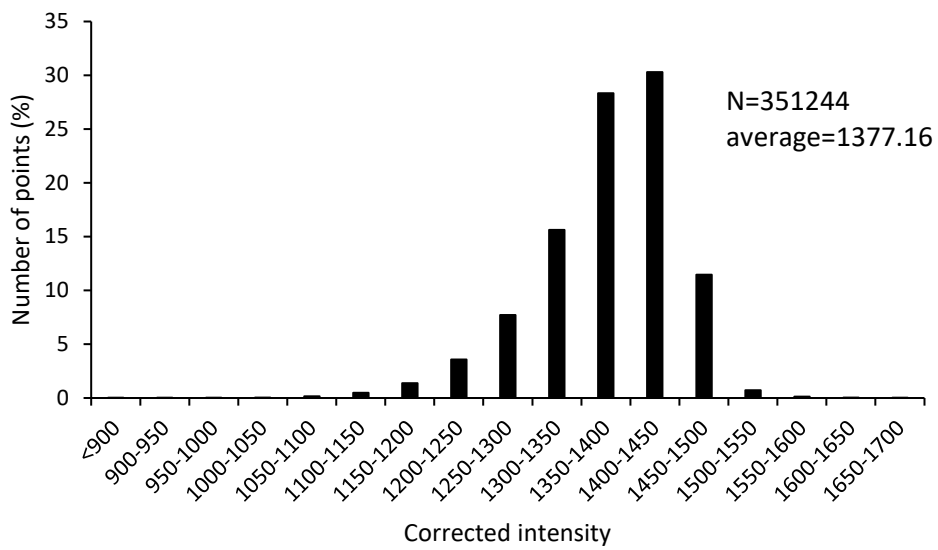

Figure A.4 Corrected intensity distribution (Site 2)

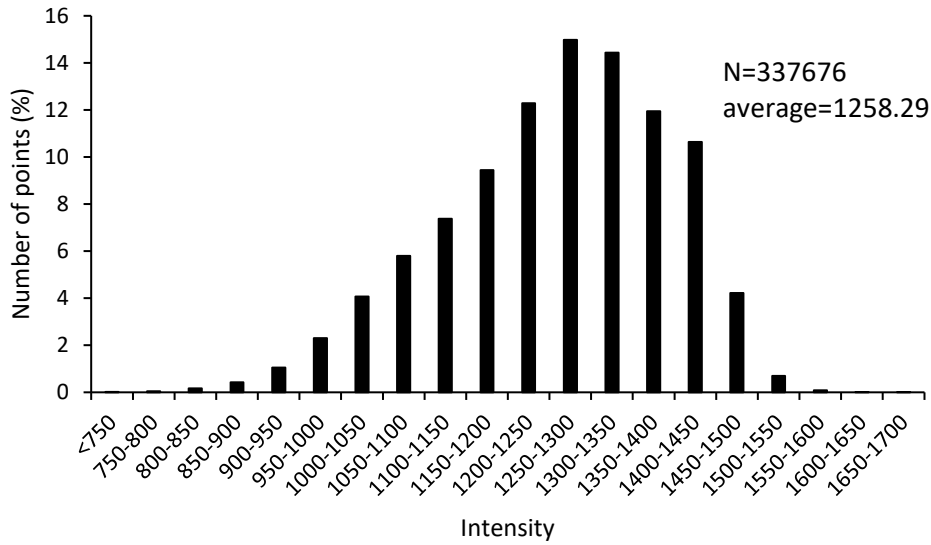

Figure A.5 Raw intensity distribution (Site 3)

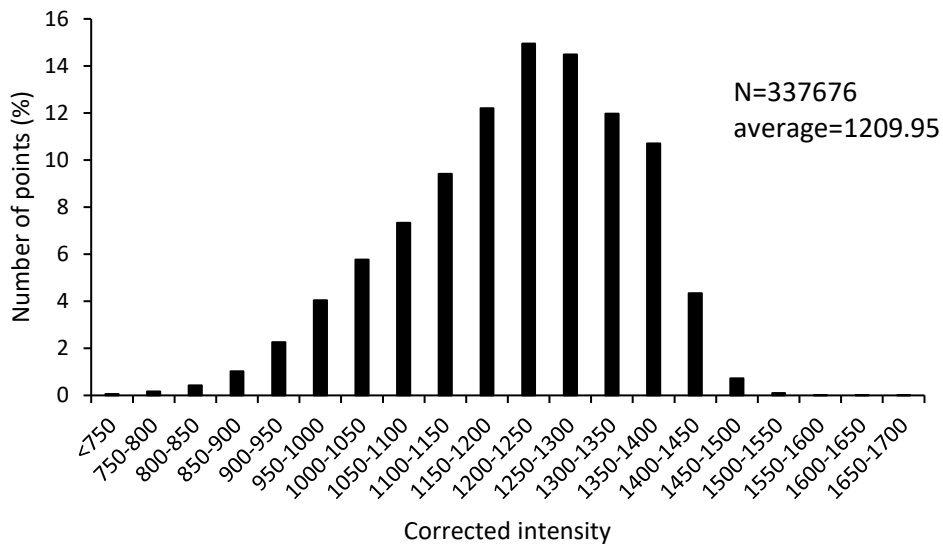

Figure A.6 Corrected intensity distribution (Site 3)

초 록

RMR을 산정하기 위해 사용되는 여러 인자 중 불연속면의 틈새, 풍화도 등을 포함하는 불연속면 상태는 가장 큰 비중을 차지한다. 암반 분류를 위한 또 다른 방식인 GSI 산정에 있어서도 joint alteration factor, 즉 불연속면의 풍화도, 충진물 상태 등 불연속면 상태 지수는 joint condition factor를 최대 10배 증가시킬 만큼 다른 어떤 지수보다 그 영향력이 크다. 기존 수기로 많이 진행되던 암반 분류가 photogrammetry, LiDAR 등의 기술 발전으로 자동화 되고 있는 추세이다. 그 중 LiDAR를 이용해 암반 분류를 함에 있어 joint spacing, waviness, smoothness 등은 정량적인 점군의 좌표를 이용해 얻는 연구가 이루어진 바 있으나 joint alteration factor를 산정하는 작업은 보다 주관적으로 산정 시 어려움이 존재했다.

앞서 말했듯이 joint alteration factor가 전체 GSI에 미치는 영향은 크므로, 따라서 LiDAR를 이용해 이를 보다 hand mapping에 가까워지게 구하는 방법에 대해 연구하였다. 기존 연구들을 통해 LiDAR의 반사 강도는 단단하고 풍화가 덜 된 암반에 대해서는 그 값이 크고 많이 풍화되고 약해진 암반에 대해서는 그 값이 작음을 알 수 있었다. 따라서, 여러 실내 실험을 통해 LiDAR에 직접적으로 영향을 미치는 인자를 산정하고 그 중 암반 풍화도와는 직접적으로 관련 없는 인자는 보정해 LiDAR 반사 강도를 이용해 joint alteration factor를 구하는 방법을 연구했다. LiDAR intensity에 직접적인 영향을 주는 인자로 주사 거리, 입사각, 거칠기, 사포를 이용한 미세 거칠기, RGB 색상 값, 암석 기본 물성 (UCS, 탄성파 속도, 공극률), 암석을 이루는 광물 조성, 포화도를 선정하고 얼마나 영향을 미치는지 고찰하기 위해 일련의 실내 실험을 수행했다. LiDAR 반사 강도에

가장 영향을 많이 미치는 요인들인 주사 거리, 입사각, RGB 색상 값을 보정해 반사 강도와 joint alteration factor의 직접적인 관계를 산정했다.

틈새 간격, 충진물의 종류 역시 반사 강도에 많은 영향을 미치는데, 실내에서 틈새를 1 mm부터 6 mm까지 1 mm 간격으로 늘려가며 반사 강도의 변화를 측정했고 충진물로 bentonite, sand를 사용해 각각 intensity에 어떤 영향을 미치는지 살펴보았다. 실험 결과 틈새나 충진물 구간에서 반사 강도가 변하는 정도를 통해 어떤 충진물이 이용되었는지 추측할 수 있다는 결론을 내렸다.

불연속면의 변질도가 다른 세 암반 사면을 LiDAR로 스캔하고 그 반사 강도를 얻어 앞서 언급한 인자들을 보정했다. 그 결과를 hand mapping을 통해 얻은 불연속면 변질도와 비교해본 결과 반사 강도는 불연속면 변질도를 범위로 산정하기에 충분했다.